Plan for particle image velocimetry measurements of flow around a model of an escort tug

Molyneux, W. D.

Publisher's version / Version de l'éditeur:
https://doi.org/10.4224/8894866
Technical Report (National Research Council of Canada. Institute for Ocean Technology); no. TR-2005-15, 2005

DOCUMENTATION PAGE

REPORT NUMBER	NRC REPORT NUMBER	DATE		
TR-2005-15		October 2005		
REPORT SECURITY CLASSIFICATION		DISTRIBUTION		
Unclassified		Unlimited		
TITLE				
PLAN FOR PARTICLE IMAGE VELOCIMETRY MEASUREMENTS OF FLOW AROUND A MODEL OF AN ESCORT TUG				
AUTHOR(S)				
David Molyneux				
CORPORATE AUTHOR(S)/PERFORMING AGENCY(S)				
Institute for Ocean Technology, National Research Council, St. John's, NL				
PUBLICATION				
SPONSORING AGENCY(S)				
Institute for Ocean Technology, National Research Council, St. John's, NL				
IOT PROJECT NUMBER		NRC FILE NUMBER		
42_2072_10				
KEY WORDS		PAGES	FIGS.	TABLES
Particle Image Velocimetry (PIV), CFD, flow		iv, 45	36	6

SUMMARY

Escort tugs are a relatively recent development within the marine industry. Their role is to control a loaded oil tanker in the event of a failure of its propulsion or steering system. The maximum speed at which an escort tug can take control of the tanker is approximately 10 knots. In order to generate the highest possible towline force at this speed (up to two and one half times the bollard pull), the tug skipper uses the combination of high yaw angle and vectored propulsion system force. These conditions are typically considered to be 'off-design' for ships and so little information is known about the hydrodynamics of this situation. The current generation of escort tugs have evolved from practical experience rather than a detailed analysis of the hydrodynamics of the situation. As a result, it is unlikely that tug performance has reached its peak.

This report presents some preliminary CFD predictions for the flow around an escort tug and the resulting forces. The report also presents a plan for carrying out Particle Image Velocimetry (PIV) experiments to measure the flow patterns around an escort tug model, based on experience gained with preliminary experiments. The report also discusses the theory of PIV methods and the associated uncertainty of PIV experiments, and what steps will need to be taken to define the uncertainty of the Memorial University PIV system.

The outcome of the research will be a unique data set of flow measurements around a yawed hull, where the yaw angle is a required operational condition. The experiment results will be used for understanding the factors effecting escort tug hydrodynamics and for validation of commercial CFD codes for the same flow situations. The validated code will be used to analyze additional hull form configurations and can be used to develop the next generation of escort tugs from sound hydrodynamic principles.

ADDRESS

National Research Council
Institute for Ocean Technology
Arctic Avenue, P. O. Box 12093
St. John's, NL A1B 3T5
Tel.: (709) 772-5185, Fax: (709) 772-2462

National Research Council Canada
Conseil national de recherches Canada

Institute for Ocean Technology
Institut des technologies océaniques

PLAN FOR PARTICLE IMAGE VELOCIMETRY MEASUREMENTS OF FLOW AROUND A MODEL OF AN ESCORT TUG

TR-2005-15

David Molyneux

October 2005

TABLE OF CONTENTS

LIST OF TABLES

Page

LIST OF FIGURES

Page

PLAN FOR PARTICLE IMAGE VELOCIMETRY MEASUREMENTS OF FLOW AROUND A MODEL OF AN ESCORT TUG

INTRODUCTION

Escort tugs are a relatively recent development within the marine industry. Their role is to control a loaded oil tanker in the event of a failure of its propulsion or steering system. The maximum speed at which an escort tug can take control of the tanker is approximately 10 knots. In order to generate the highest possible towline force at this speed (up to two and one half times the bollard pull), the tug skipper uses the combination of high yaw angle and vectored propulsion system force. These conditions are typically considered to be ‘off-design’ for ships and so little information is known about the hydrodynamics of this situation. The current generation of escort tugs have evolved from practical experience rather than a detailed analysis of the hydrodynamics of the situation. As a result, it is unlikely that tug performance has reached its peak.

This report presents some preliminary CFD predictions for the flow around an escort tug and the resulting forces. The report also presents a plan for carrying out Particle Image Velocimetry (PIV) experiments to measure the flow patterns around an escort tug model, based on experience gained with preliminary experiments. The report also discusses the theory of PIV methods and the associated uncertainty of PIV experiments, and what steps will need to be taken to define the uncertainty of the Memorial University PIV system.

The outcome of the research will be a unique data set of flow measurements around a yawed hull, where the yaw angle is a required operational condition. The experiment results will be used for understanding the factors effecting escort tug hydrodynamics and for validation of commercial CFD codes for the same flow situations. The validated code will be used to analyze additional hull form configurations and can be used to develop the next generation of escort tugs from sound hydrodynamic principles.

OPERATING CONDITIONS AND DESIGN VARIABLES

The principal operational requirement for an escort tug is to be able to bring a loaded oil tanker to a controlled stop in the event of a steering or propulsion system failure on the tanker. The tug must be able to do this up to a maximum tanker speed of approximately 10 knots. The force required to control the tanker is generated by the tug using a combination of yaw angle (typically between 35 and 55 degrees) and azimuthing thruster angle (relative to the centreline of the tug). Using this approach it is possible to generate a force with a magnitude of up to two and a half times the bollard pull of the tug. The resulting force and its angle of application depend on the speed of the tanker, the delivered power of the tug and the direction of the thrusters on the tug. A popular and reliable choice of propulsion system for escort tugs is twin vertical axis propellers, which give very flexible control over the level of thrust and its direction. These propellers are typically fitted inside a protective cage. The profile of such a tug is shown in Figure 1.

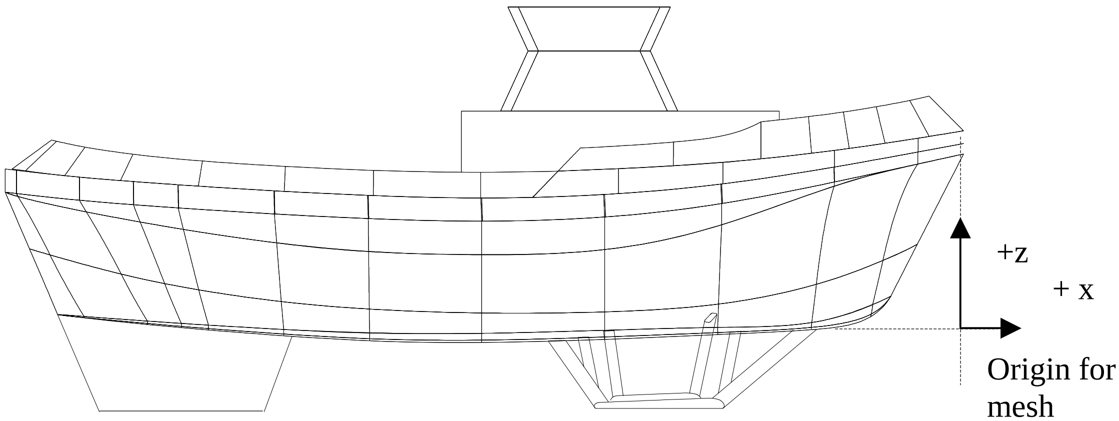

Figure 1, Side view of VSP tug (Tug B), fitted with vertical axis propellers, showing low aspect ratio fin (Fin 1) and propeller protection cage

At 10 knots, in indirect mode, maximum steering force and maximum braking force are generated with the hull at yaw angles between 35 and 55 degrees. The major difference between the two conditions is the orientation of the thrusters. In either case, the hydrodynamic force normal to the tug's centerline is the largest force component and is about an order of magnitude larger than the longitudinal force (Molyneux 2002). Figure 2 shows side force coefficient, Cq, against yaw angle, for two escort tug models, Tugs A and B, with different fin and keel options (Molyneux, 2002). Tug B is shown above and Tug A was an azimuthing stern drive tug with a box keel.

Figure 2 shows two distinct peaks in the side force coefficient for all cases of the hull combined with a fin or box keel. The main peak occurs between 90 and 105 degrees yaw, but there is a clear secondary peak between 35 and 40 degrees yaw. It appears that the smaller peak is reached when the flow on the fin or keel stalls and the level of lift generated by the fin starts to reduce but there is no flow visualization data to confirm this assumption. It also is reasonable to assume that the main peak was caused by the pressure drag of the hull at its maximum projected area. From Figure 2, it can be seen that the level of force generated by the fin or box keel is about half of the total hydrodynamic force and as a result it is an essential contribution to the overall performance of the tug.

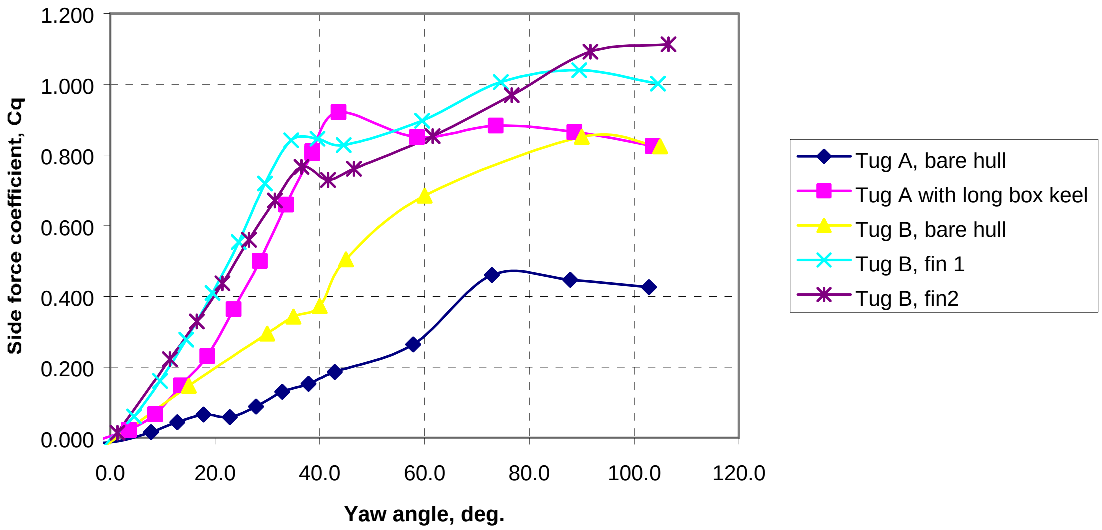

Figure 2, Variation of side force coefficients for escort tug hulls with yaw angle (propellers or z-drives removed)

An important test for the validity of applying CFD to the design of escort tugs was to predict the force coefficients shown in Figure 2. The forces result from potentially complex interactions between flow around a low aspect ratio fin at a high angle of attack, and flow around a wide, shallow hull at a high yaw angle.

The tugs discussed above had waterline lengths between 38m and 40m. A tanker speed of 10 knots is equivalent to a Froude number of approximately 0.26 for the tug. At 8 knots the Froude number is approximately 0.21. At 6 knots (the limit at which force data was obtained for all yaw angles) the resulting Froude number was 0.16. At the two lower Froude numbers, the resulting waves generated by the hull should be quite small. Observations made during the experiments discussed above confirm this, although no measurements of wave amplitude were made. Given this observation, ignoring the effects of the free surface on the flow patterns and the forces generated should not introduce a significant error when making preliminary calculations.

HYDRODYNAMIC FORCES AND FLOW PATTERNS AROUND AN ESCORT TUG PREDICTED WITH CFD

Hullform Configuration and Mesh Design

For an escort tug, the fin has a very large effect on the total force but the effect of different shaped fins is much smaller, once allowance has been made for the area of the fin. This is illustrated in Figure 2 (Molyneux, 2002). The key factor to reproduce in the CFD results is the effect of the fin or keel on the forces generated by the tug. The test cases considered for initial CFD predictions of flow patterns and forces was Tug B, with Fin 1 (shown in Figure 1) and Tug B with no fin. In each case the protective cage was removed. A summary of the principal dimensions for the tug model is given in Table 1.

The fin was at the upstream end of the hull, for all cases when it was fitted. The hull remained in the same orientation when the fin was removed.

Length, waterline, m	2.122
Beam, waterline, m	0.789
Draft, hull, m	0.211
Daft, maximum, m	0.471
Displacement, kg	213.3
Nominal scale	1:18

Table 1, Summary of model particulars

Meshing was carried out using *GAMBIT 2.1*. The surfaces used to the construct the 1:18 scale physical model (Molyneux, 2002) were trimmed to the nominal waterline. The trimmed surfaces were imported as IGES files and cleaned up using the utilities available within *GAMBIT*. The origin for the original surfaces was on the centreline, at the level of the keel, with the longitudinal position given by at the extreme aft end of the hull (above the waterline), shown in Figure 1. This point was retained as the origin for the mesh. Two volumes were created around the hull. The inner volume, close to the hull had a constant mesh size at all the boundaries. The outer volume had larger mesh elements at the outer surface than the inner surface. The mesh geometry is shown plotted in Figure 3, for the tug with fin. The overall mesh geometry was the same for the tug with no fin.

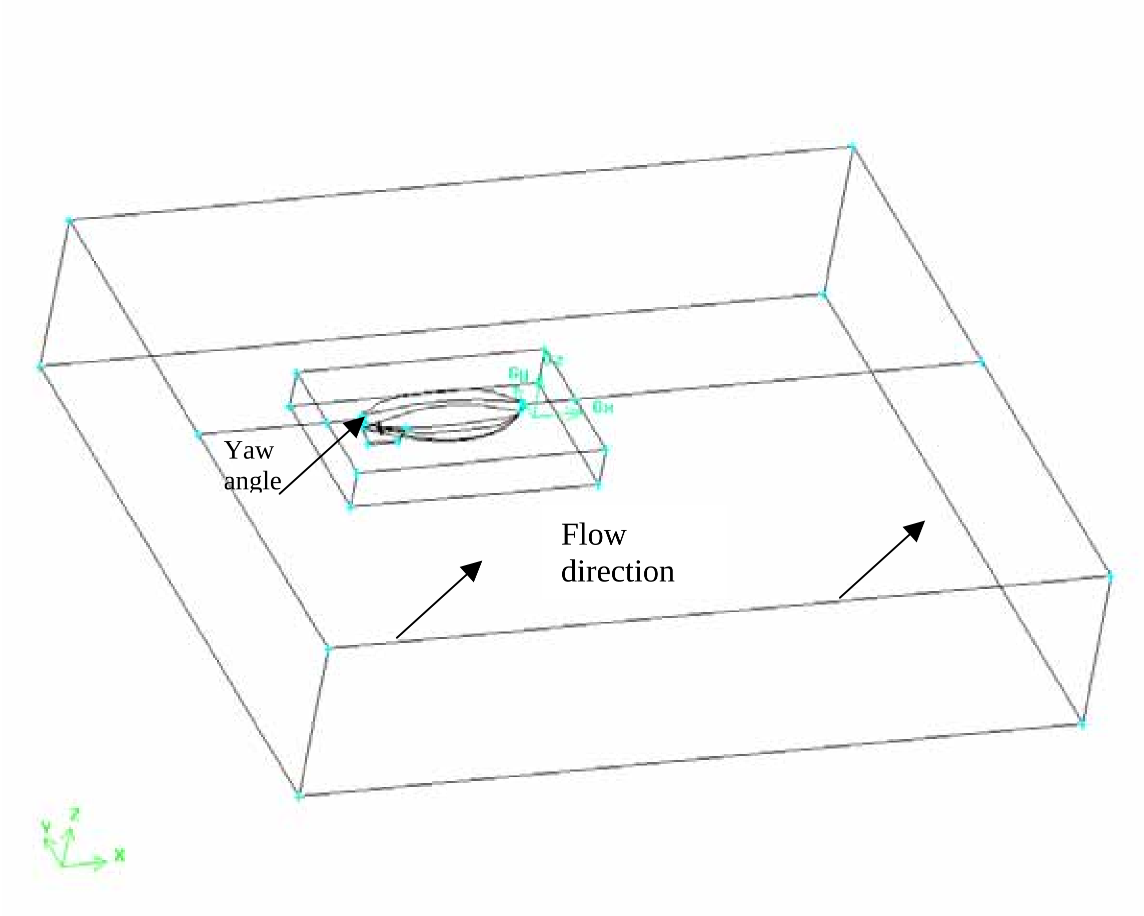

Figure 3, Scope of mesh and flow direction (shown for tug with fin)

The resulting volume was meshed with unstructured, tetrahedral elements. A tetrahedral mesh was chosen, since the hull shape was quite complex and the amount of time to carry out the simulations was relatively limited. The same mesh size at the boundaries was used for the case with the fin and without the fin.

A summary of the mesh is given in Table 2. Dimensions for the surfaces were originally given in inches at model scale. The mesh was re-scaled in *FLUENT* to have units of metres, model scale. All dimensions given in this report are metres, model scale.

	x max m	x min m	y max m	y min m	z max m	z min m	mesh size* m	Number of elements
Inner mesh	0.508	-2.667	1.016	-1.016	0.211	-0.297	0.03175	482,260
Outer mesh	5.715	-4.318	4.318	-4.318	0.211	-1.948	0.1016	1,688,639

* at surface

Table 2, Summary of mesh dimensions

Boundary conditions were set as velocity inlets on the two upstream faces, and pressure outlets at the two downstream faces. The upper and lower boundaries were set as walls with zero shear force. The hull surface was set as a no-slip wall boundary condition.

The mesh at the hull and waterline boundary is shown in Figure 4 and 5 for the case without a fin and Figure 6 and 7 for the case with the fin.

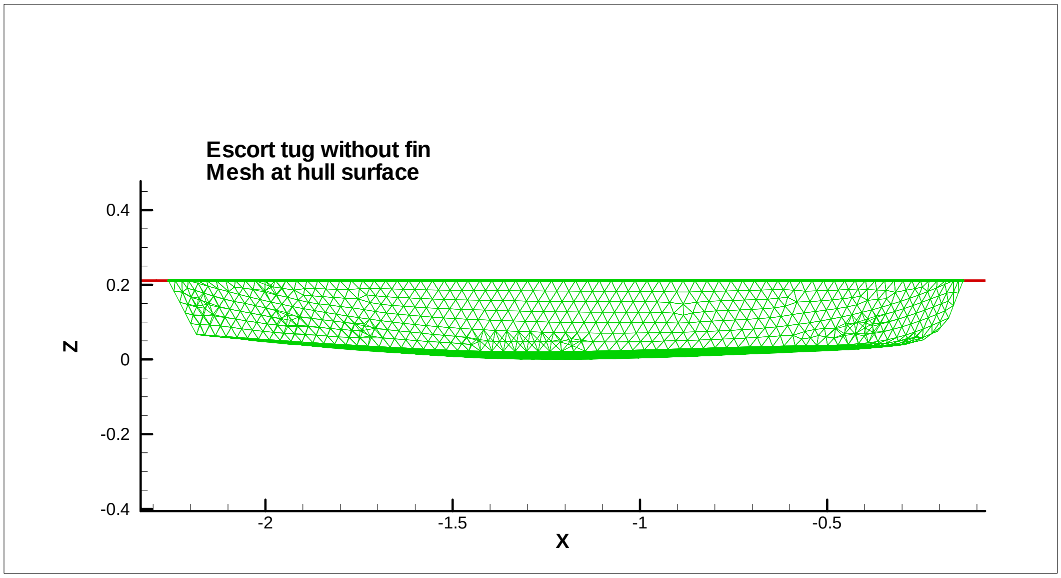

Figure 4, Tetrahedral mesh for escort tug, without fin, profile view

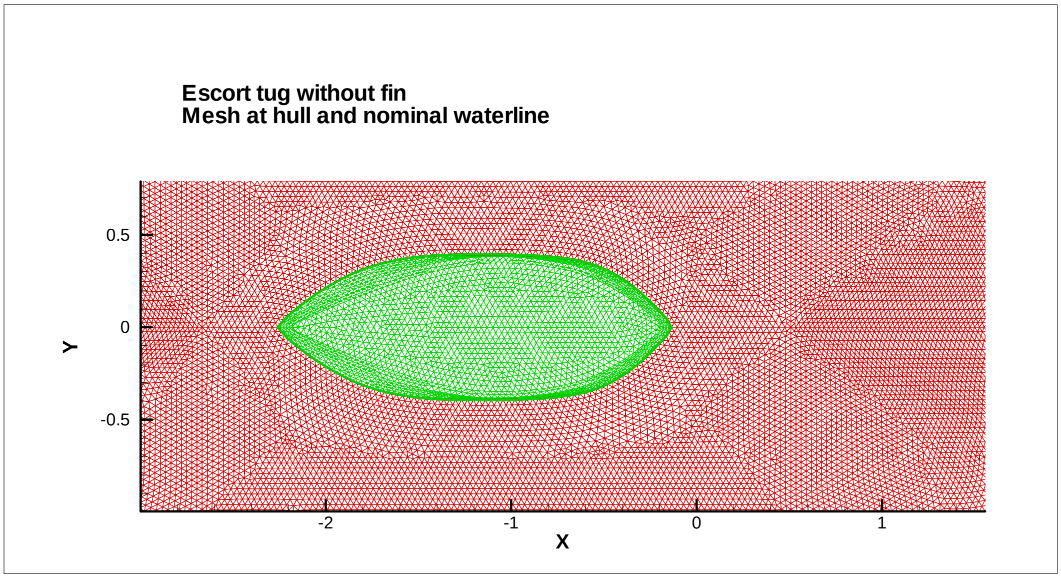

Figure 5, Tetrahedral mesh for escort tug, without fin, waterline view

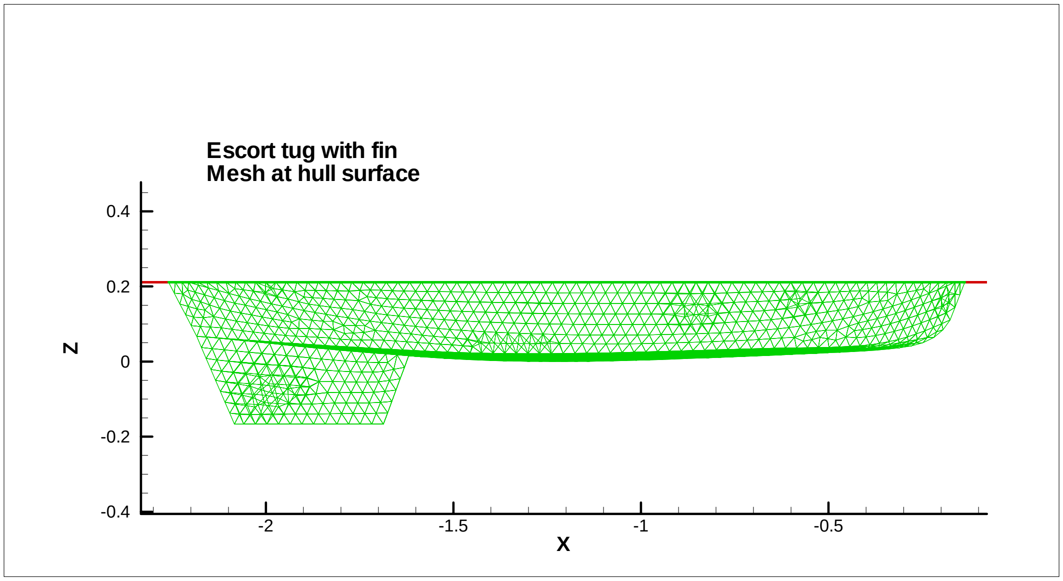

Figure 6, Tetrahedral mesh for escort tug, with fin, profile view

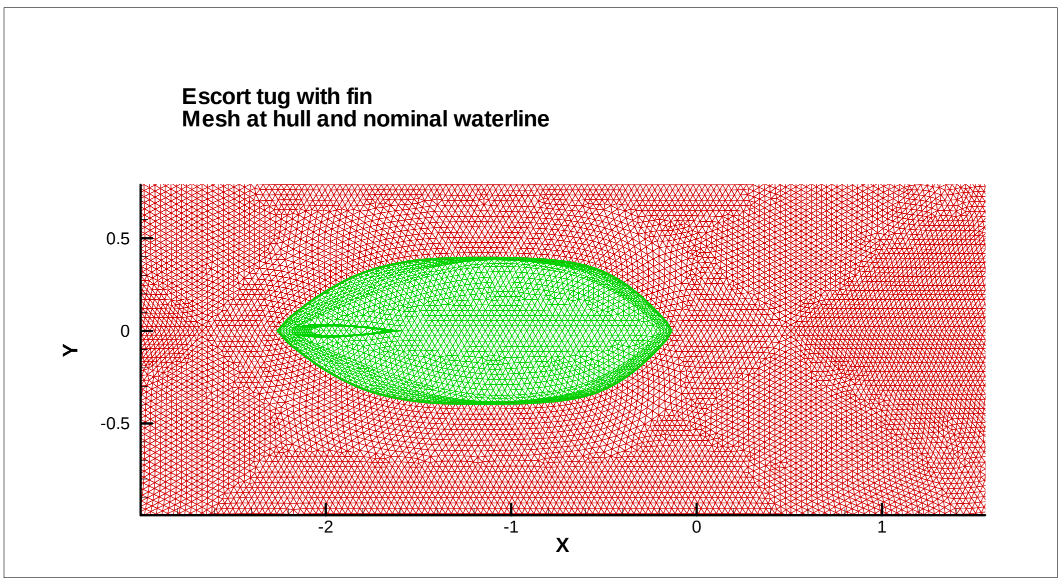

Figure 7, Tetrahedral mesh for escort tug, with fin, waterline view

CFD SOLVER

The CFD solver used was *FLUENT 6.1.22*. Uniform flow entered the domain through a velocity inlet on the upstream boundaries and exited through a pressure outlet on the downstream boundaries. The hull surface was defined as a no-slip wall and the waterline was defined as a slip wall. Flow speed magnitude was set at 0.728 m/s, which corresponded to 6 knots at 1:18 scale, based on Froude scaling. The fluid used was fresh water.

The angle between the incoming flow and the hull (yaw angle) was set by adjusting the boundary conditions, so that the velocity at the inlet planes had two components. The cosine component of the angle between the steady flow and the centreline of the hull was in the positive x direction for the mesh and the sine component in the positive y direction. The pressure outlet planes were set so that the backflow pressure was also in the same direction. The advantage of this approach was that one mesh could be used for all the yaw angles. Yaw angles from 10 degrees to 45 degrees were simulated (using the same mesh) for the hull with the fin, and yaw angles from 10 to 55 degrees were simulated for the hull with no fin.

The turbulence model used was a $\kappa-\omega$ model with the default parameters. Turbulence intensity and turbulent viscosity ratios were set at 1% and 1 respectively. The flow was solved for the steady state case. The non-dimensional residual for each solution variable (continuity, x, y, and z velocity components, κ and ω) was set to 10^{-3} (default values). All flow conditions reported came to a solution within these tolerances. Results were presented as forces acting on the hull (including the fin if it was present) and as flow vectors within the fluid.

Some test cases were solved in the time domain (35 and 55 degree yaw for hull with fin), but the computed forces were within 0.6 N of the steady state case, and so this was not explored any further.

CFD SIMULATIONS OF FLOW AROUND AN ESCORT TUG

Forces on Hull

Calculated forces acting on the combined hull and fin are reported within the output from the CFD solver. Experiment data for the hull only, the hull and protective cage, and the full combination of hull, protective cage and fin were also available (Molyneux 2002). Forces were measured in the ship based axis system. Surge force was positive along the x axis and sway force was positive along the y axis (in the model-based grid reference system).

Predicted forces for each yaw angle and hull/fin combination are given in Table 3. Experiment values for the hull only condition were available for a direct comparison, and the values for the hull and fin only were estimated from the other measured data, by determining the effect of the protective cage as the difference between the hull only and the combined hull and cage condition, and subtracting this difference from the hull, cage and fin condition. This approach assumed that the interaction of the flow between the fin and the protective cage was negligible. The experiment values are compared with the CFD predictions in Figure 8 for the sway (y-direction) force component and Figure 9 for the surge (x-direction) force component.

Condition	Speed, m/s	Yaw angle, deg	# of iterations	Surge, N	Total sway, N
Hull only	0.728	10	170	5.916	8.761
Hull only	0.728	20	195	5.535	17.298
Hull only	0.728	35	225	4.262	31.250
Hull only	0.728	45	233	2.921	40.415
Hull only	0.728	55	232	1.175	48.650
Hull and fin	0.728	10	224	5.878	20.856
Hull and fin	0.728	20	259	3.752	42.822
Hull and fin	0.728	30	284	1.22	65.079
Hull and fin	0.728	35	293	0.418	75.998
Hull and fin	0.728	40	310	-0.127	84.030
Hull and fin	0.728	45	428	1.146	86.530

Table 3, Predicted forces, with and without fin

These figures show that the CFD method used predicted many of the essential features of the effect of the fin on the total hydrodynamic force generated. Sway force (y-direction) variation with yaw angle is shown in Figure 8. For the case with no fin, the predicted forces under estimated the experiment values by 0.13 N/degree yaw up to 35 degrees of yaw. Above 35 degrees, the predicted values show a similar trend to the lower values, but the experiment values show some irregularity. For the case with the fin, the forces were under predicted by the CFD method compared to the experiment values by 0.69 N/degree yaw up to yaw angles of 30 degrees. Above this value the experiment and CFD predictions become non-linear. The CFD predictions show the flattening of the sway force component above 40 degrees, even though the magnitude of the force is under-predicted by 18 percent. Below 20 degrees the agreement between the experiment values and the CFD predictions is very good.

The surge force (x-direction) component is shown in Figure 9. The agreement for the hull only condition is within 2.5N throughout the range of yaw angle. The agreement between the experiment values and the predictions for the cases when the fin was fitted was not as good (within 5 N throughout the range of yaw angle) but this is within the uncertainty of the experiment values.

Above 45 degrees, the CFD predictions for the hull with the fin did not converge to a solution within the default tolerances discussed above. Since 45 degrees is an average operating yaw angle for an escort tug, this was not considered to be a significant problem.

Overall, the agreement between the measured and predicted values was acceptable for preliminary engineering estimates of tug performance when compared to model experiments. It was unfortunate that there was no direct measurement of the case for the combined hull and fin during experiments, but the estimated values should be reasonably reliable provided the interaction between the flow around the fin and the flow around the cage is negligible.

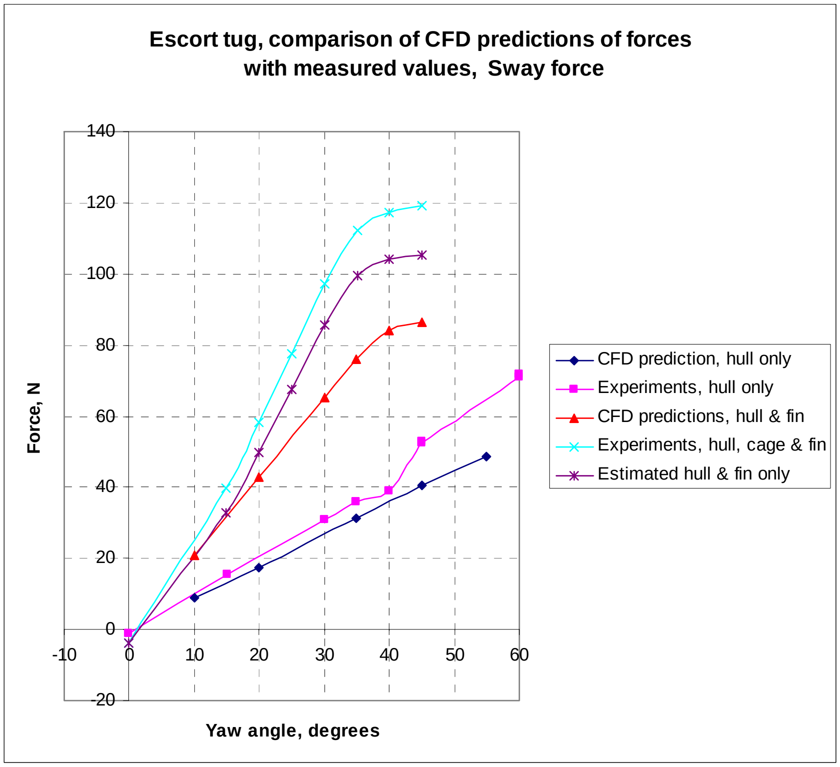

Figure 8, Comparison of predicted sway forces with measured values

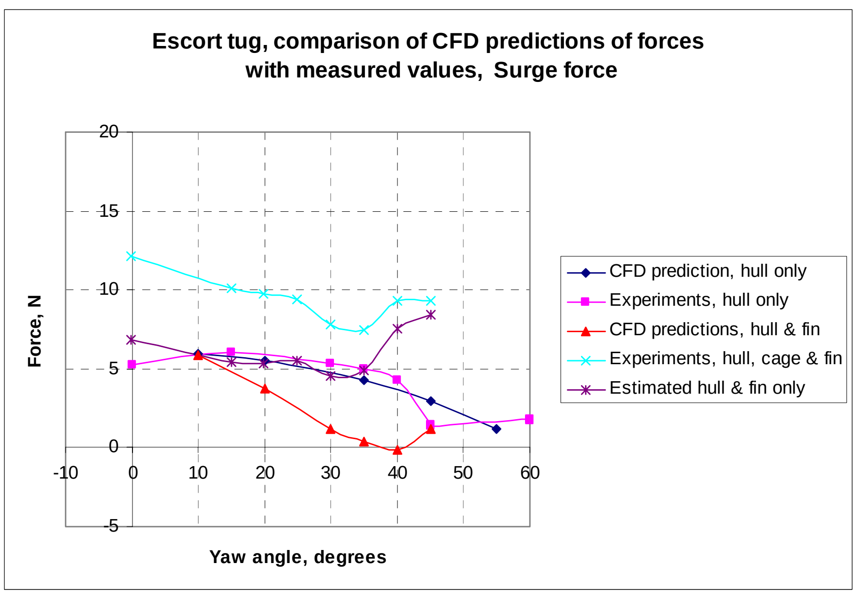

Figure 9, Comparison of predicted surge forces with measured values

Flow patterns

The CFD predictions were interpolated to obtain flow patterns at 5 stations spaced along the hull. The sections used are summarized in Table 4.

	Section	Location, m	Fraction of WL length
Fwd end of waterline		-2.259	1.000
Mid-fin section	1	-1.902	0.832
	2	-1.550	0.666
Midships section	3	-1.198	0.500
	4	-0.846	0.334
	5	-0.494	0.168
Aft end of waterline		-0.137	0.000
Waterline length, m		2.122	

Table 4, Section locations for predicted flow patterns

Four cases were selected for illustration. Two of the cases were for the hull at 20 degrees of yaw, with and without the fin. These cases were chosen since it represented the approximate limit of good agreement for the force data discussed above. It was hoped that since the forces were well predicted, the flow patterns would also be well predicted. The other cases chosen were the hull with and without fin at 45 degrees yaw. These conditions were chosen since 45 degrees was a typical yaw angle for an escort tug, and beyond the range of yaw angles analyzed for the Series 60 C_B=0.6 hull (Molyneux 2005).

CFD predictions of the flow patterns at each section, with and without the fin for a yaw angle of 20 degrees are given in Figures 10 to 19, and for a yaw angle of 45 degrees in Figures 20 to 29. The simulated flows are presented as vectors of in plane flow components (v_y and v_z) and contours of through plane flow component (v_x). Planes were interpolated at constant values of x within the mesh, and so flow direction is at a different angle to the planes for each yaw angle. The advantage of this method was that single planes could be defined within the mesh and used for all results.

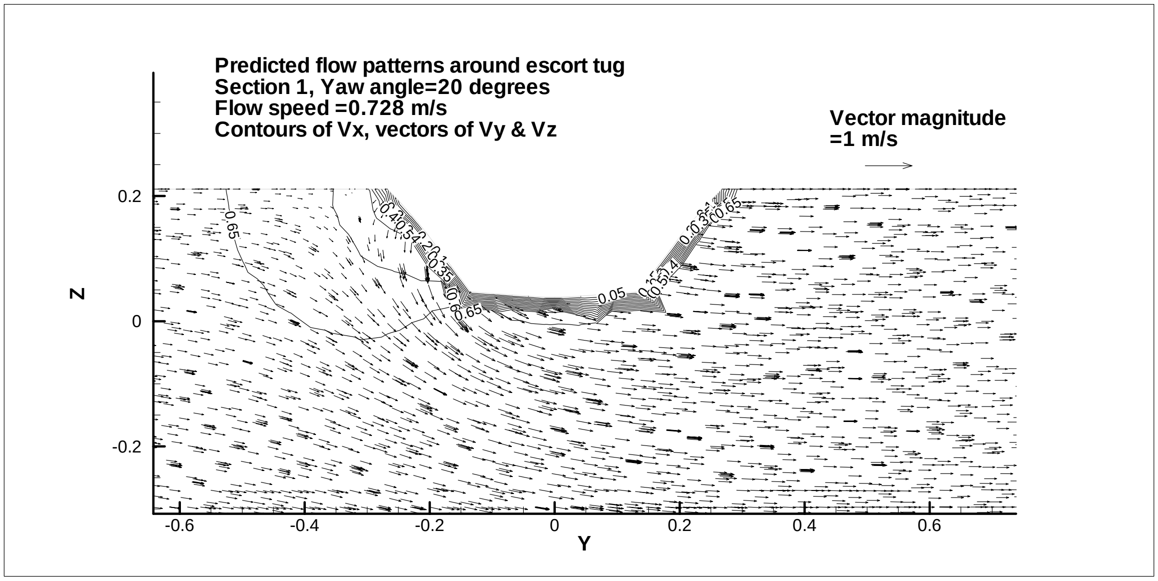

Figure 10, Yaw angle 20 degrees, without fin, section 1

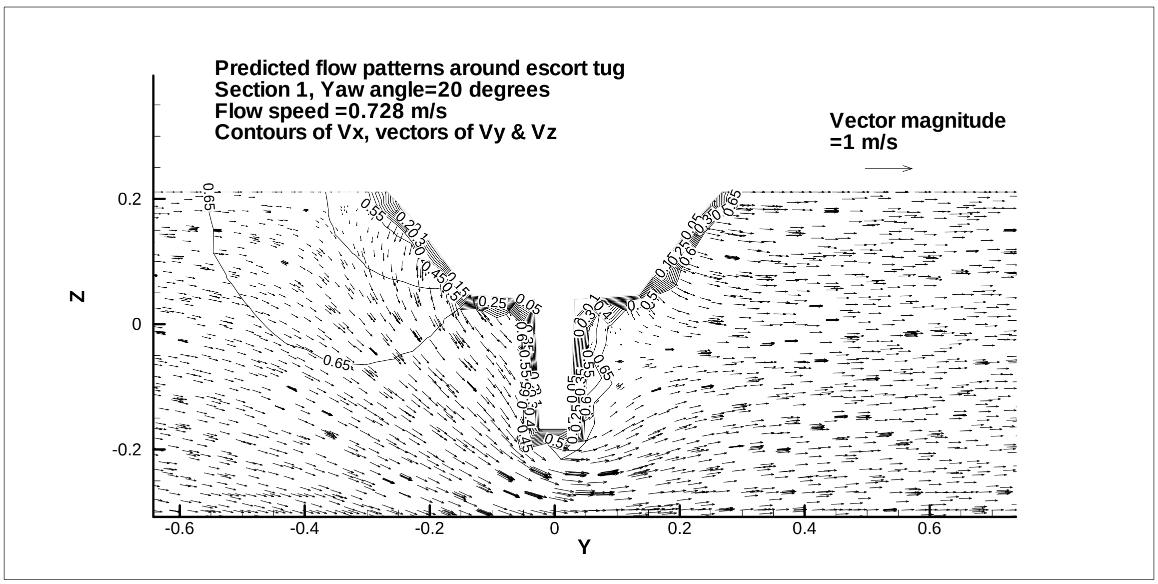

Figure 11, Yaw angle 20 degrees, with fin, section 1

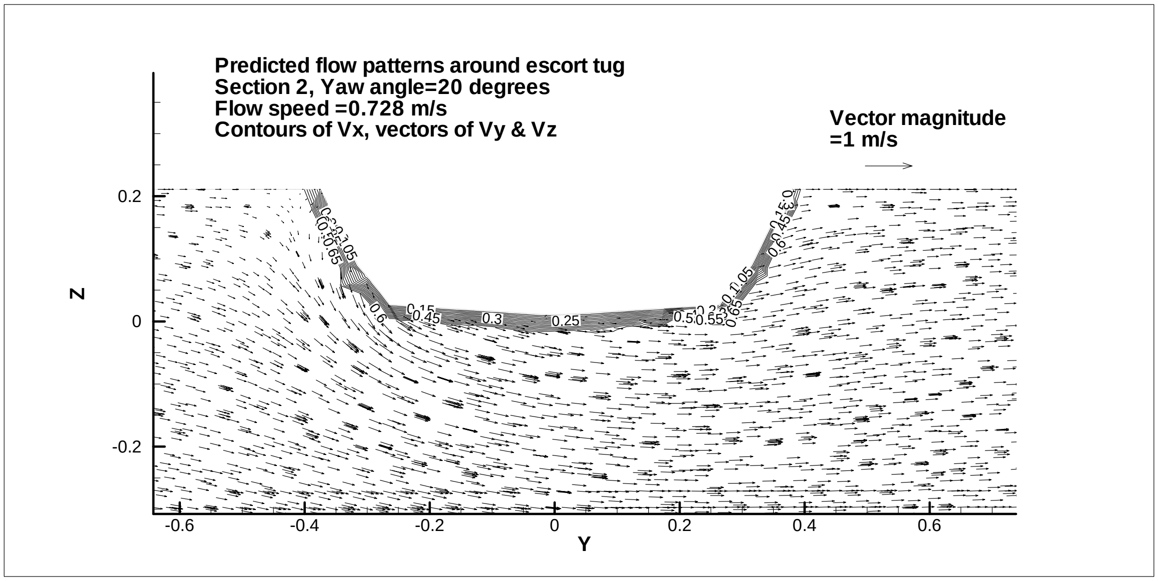

Figure 12, Yaw angle 20 degrees, without fin, section 2

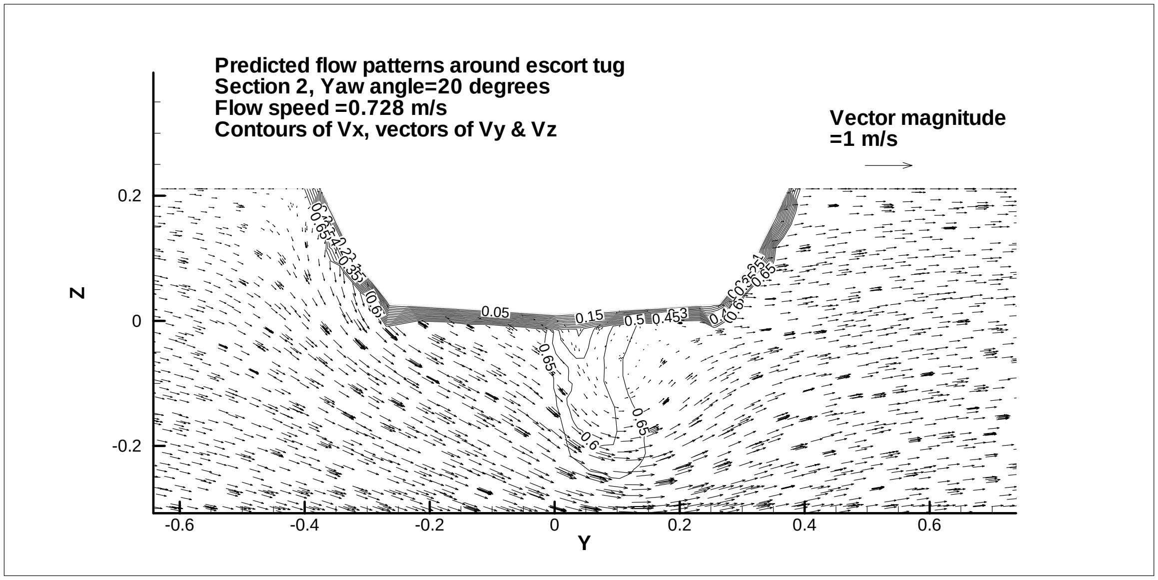

Figure 13, Yaw angle 20 degrees, with fin, section 2

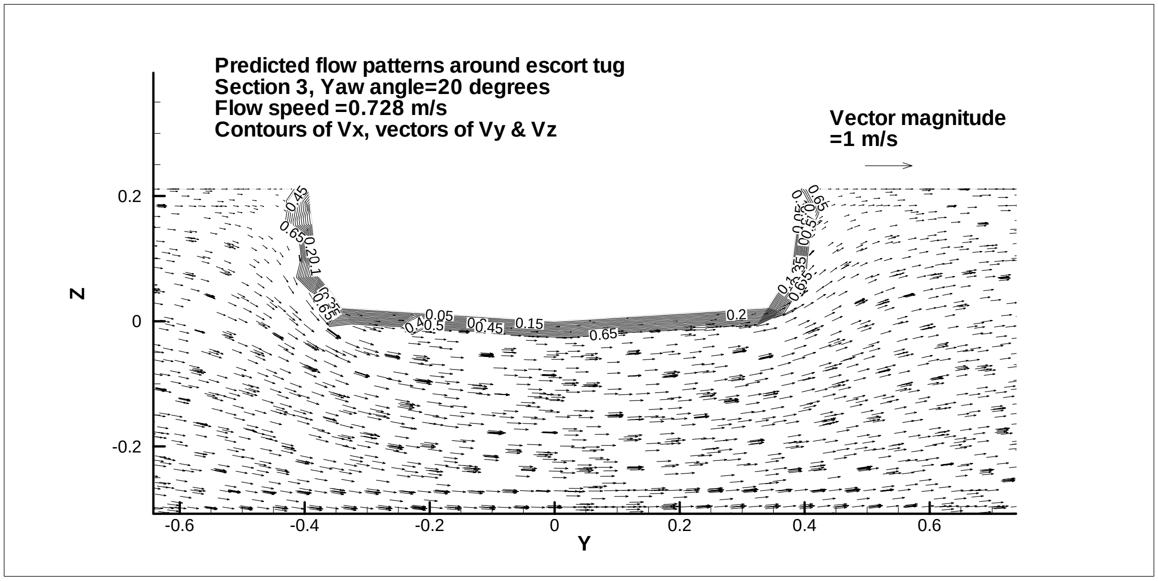

Figure 14, Yaw angle 20 degrees, without fin, section 3

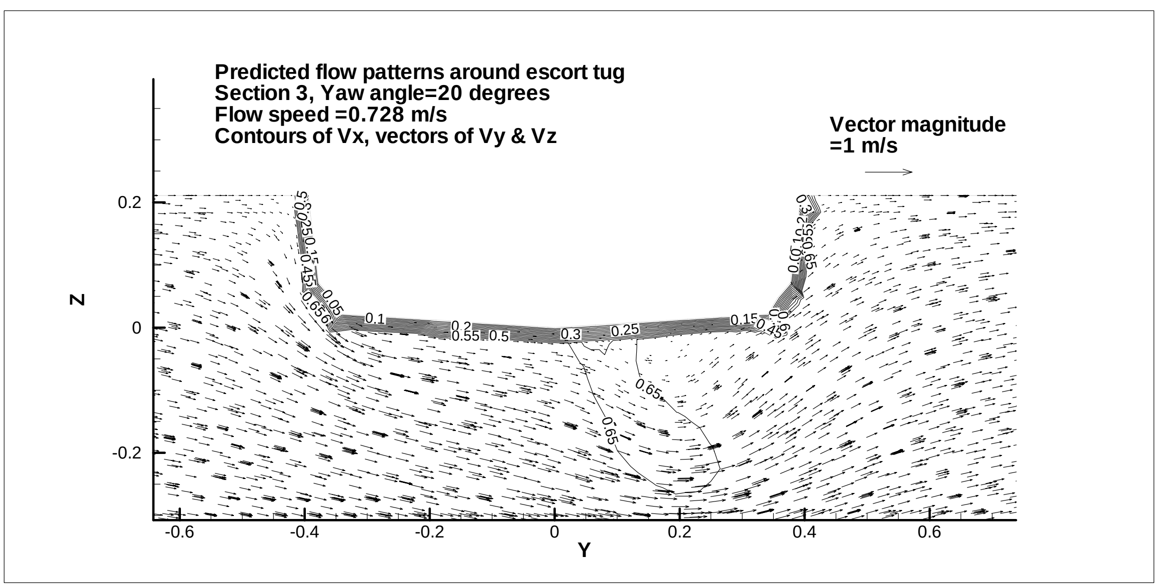

Figure 15, Yaw angle 20 degrees, with fin, section 3

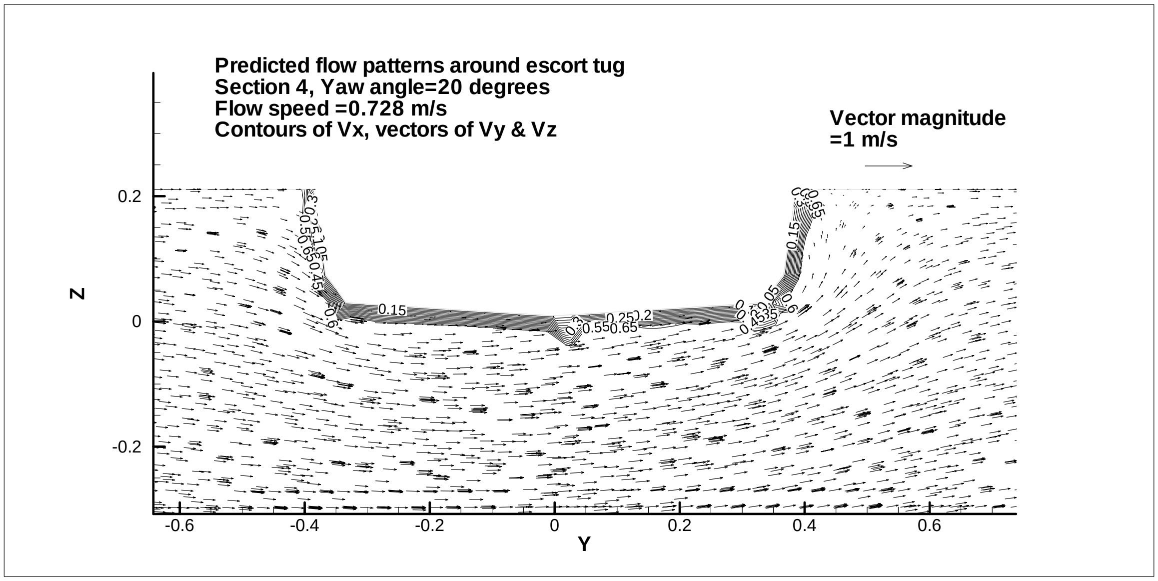

Figure 16, Yaw angle 20 degrees, without fin, section 4

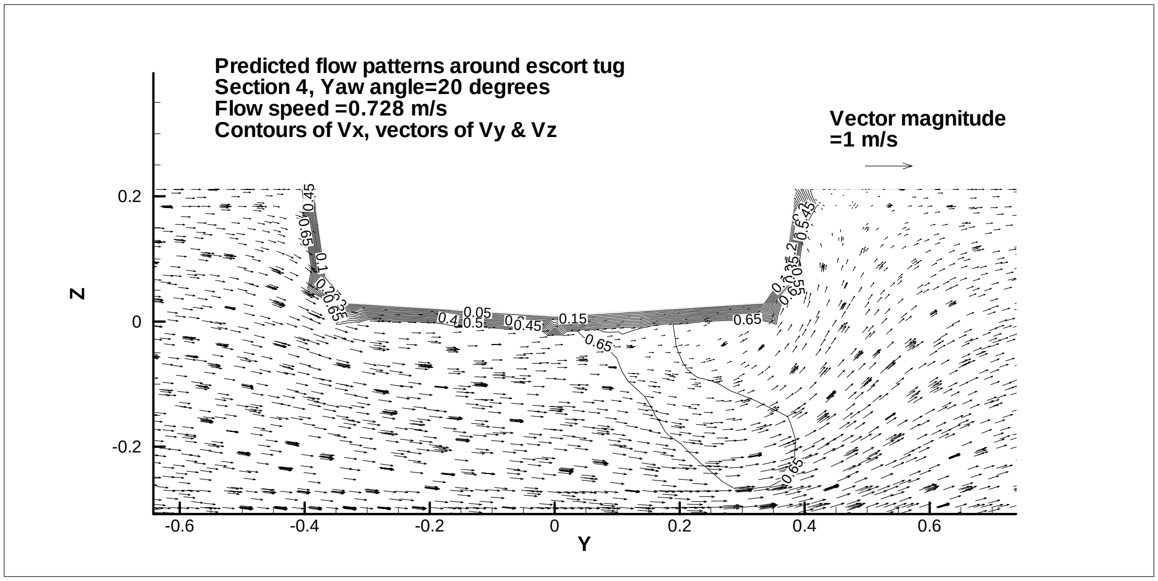

Figure 17, Yaw angle 20 degrees, with fin, section 4

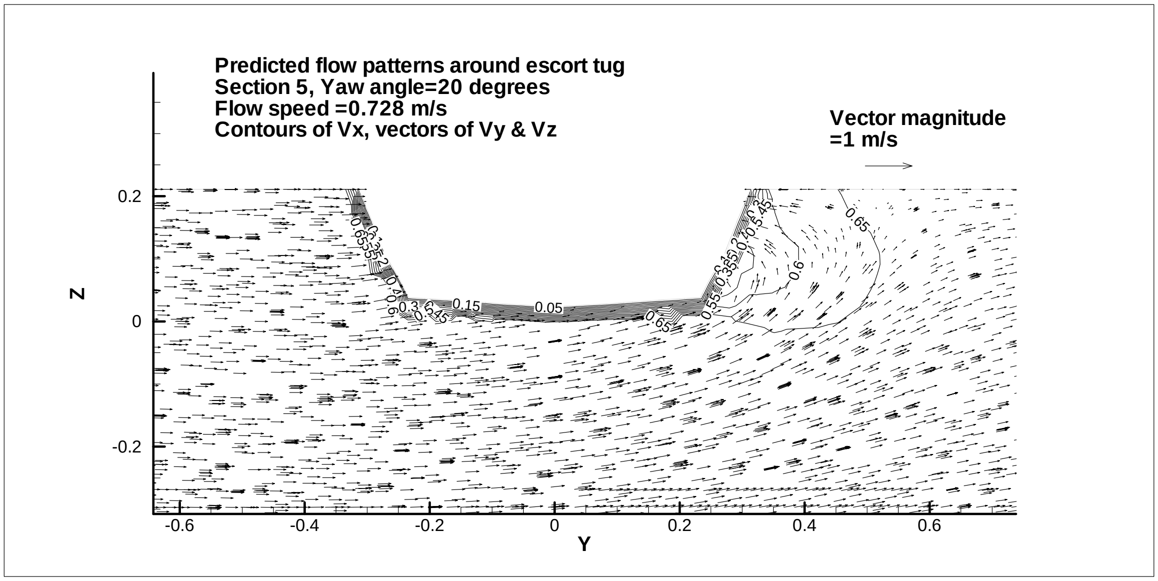

Figure 18, Yaw angle 20 degrees, without fin, section 5

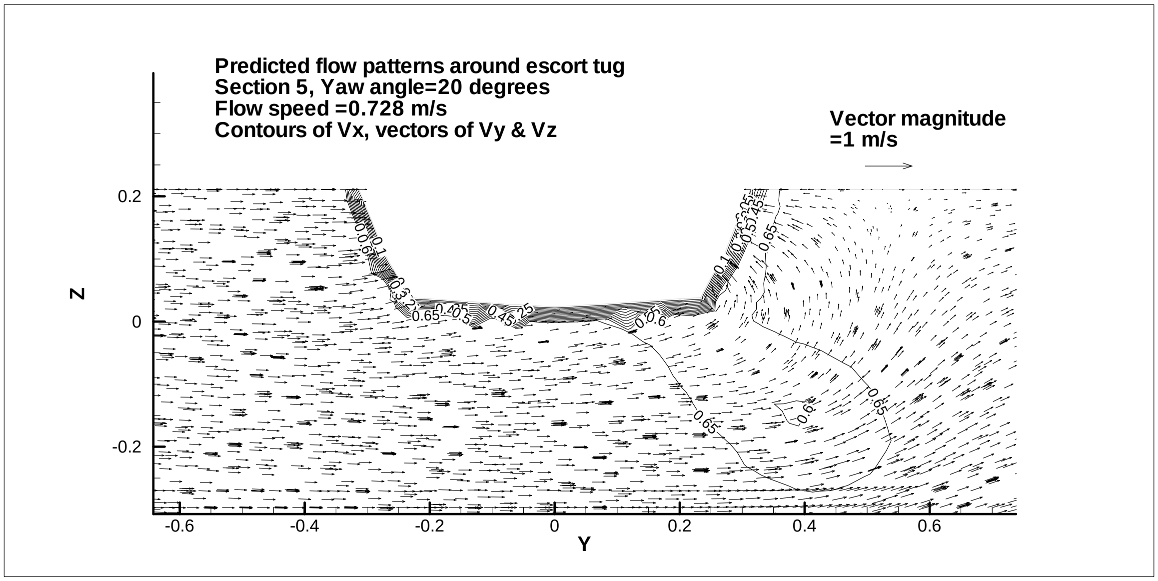

Figure 19, Yaw angle 20 degrees, with fin, section 5

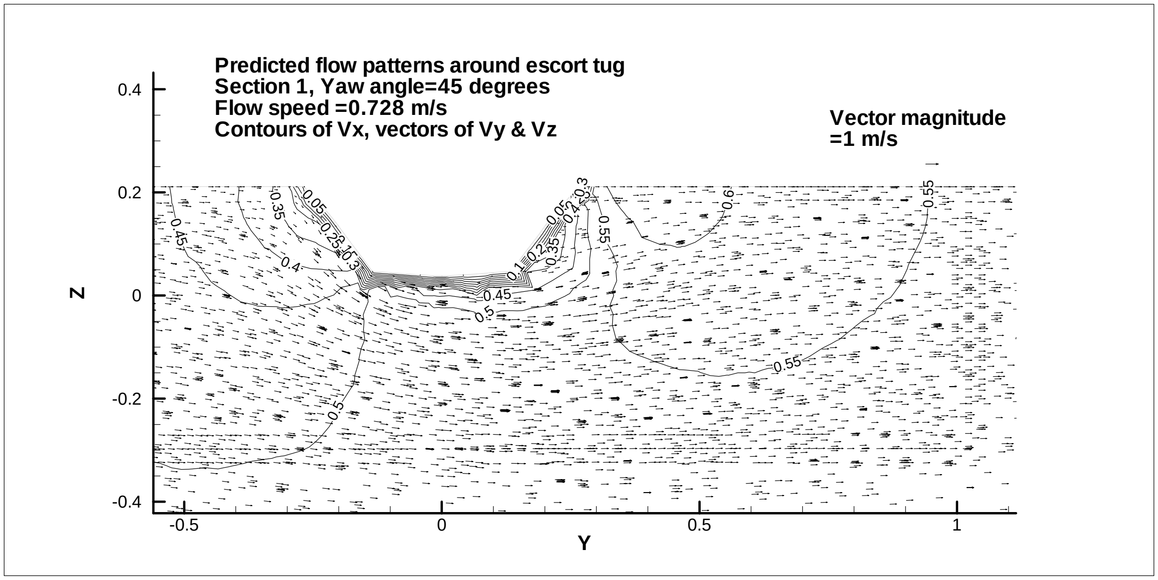

Figure 20, Yaw angle 45 degrees, without fin, section 1

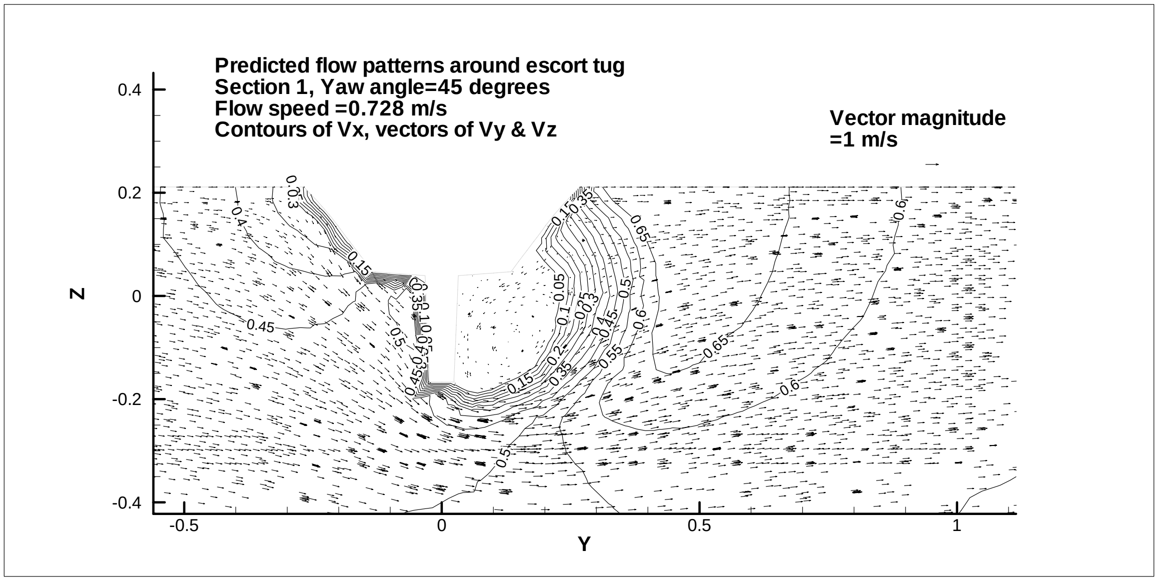

Figure 21, Yaw angle 45 degrees, with fin, section 1

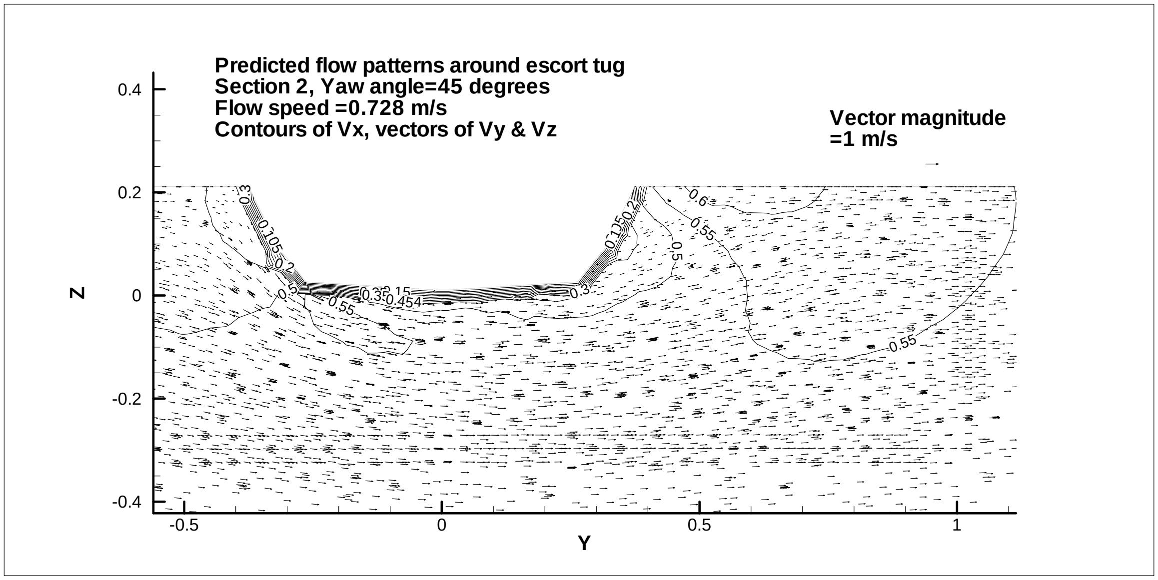

Figure 22, Yaw angle 45 degrees, without fin, section 2

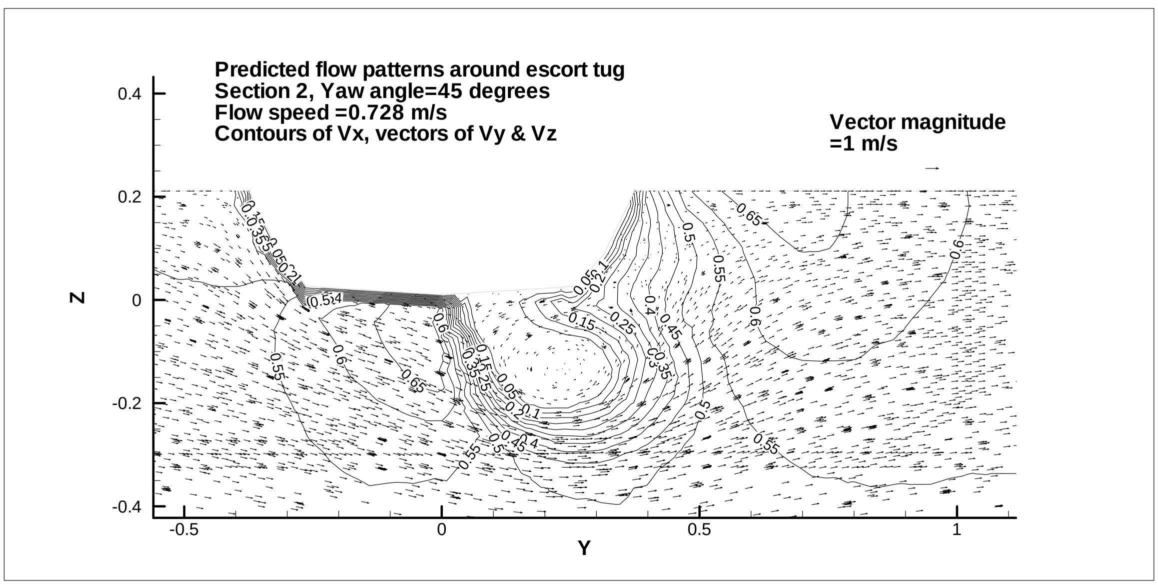

Figure 23, Yaw angle 45 degrees, with fin, section 2

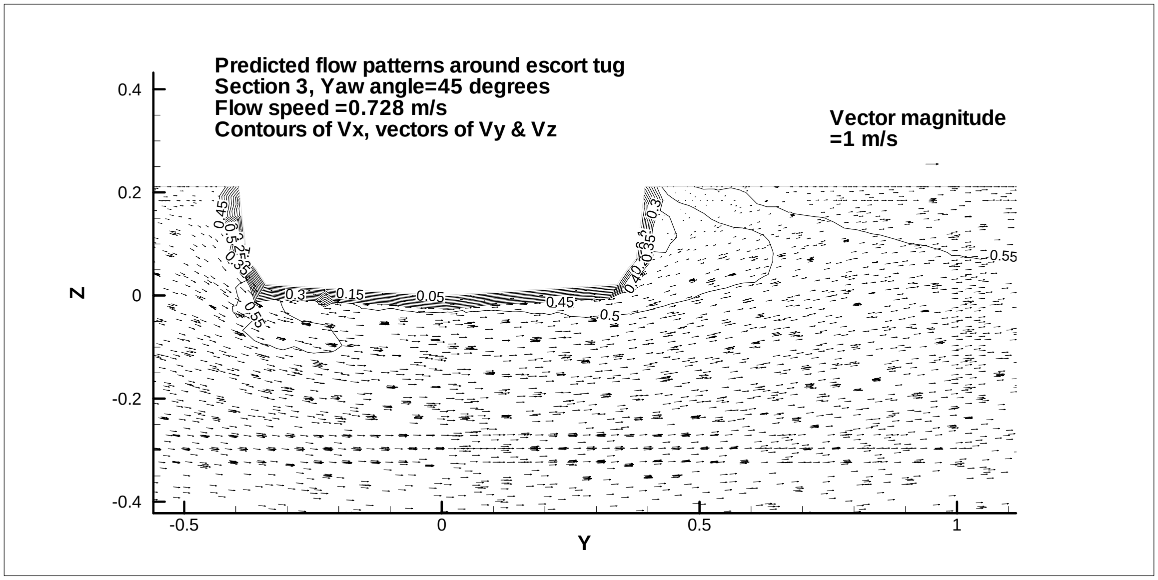

Figure 24, Yaw angle 45 degrees, without fin, section 3

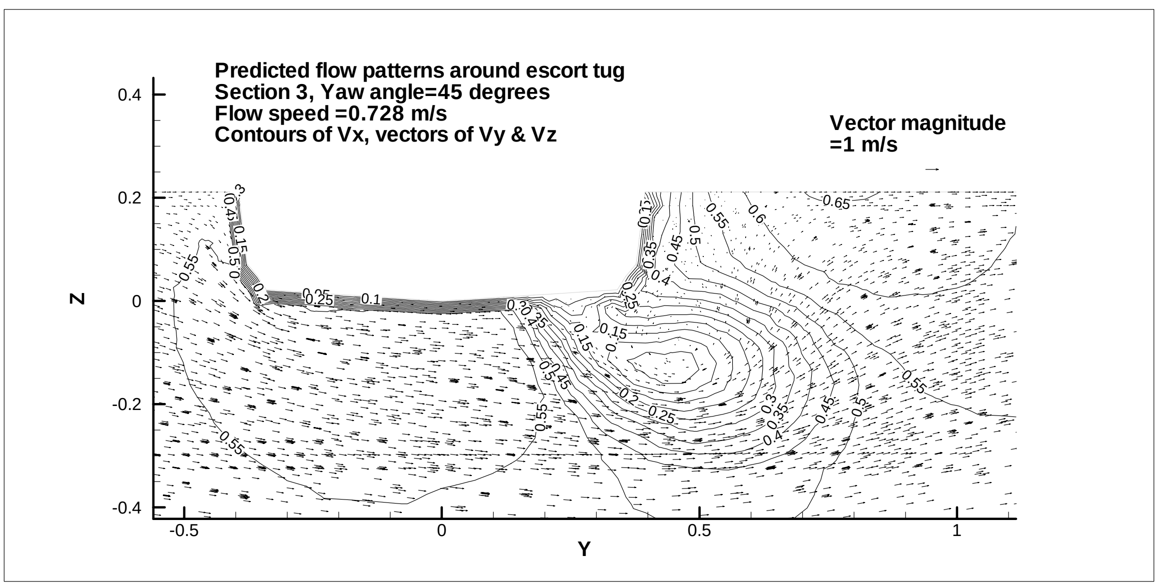

Figure 25, Yaw angle 45 degrees, with fin, section 3

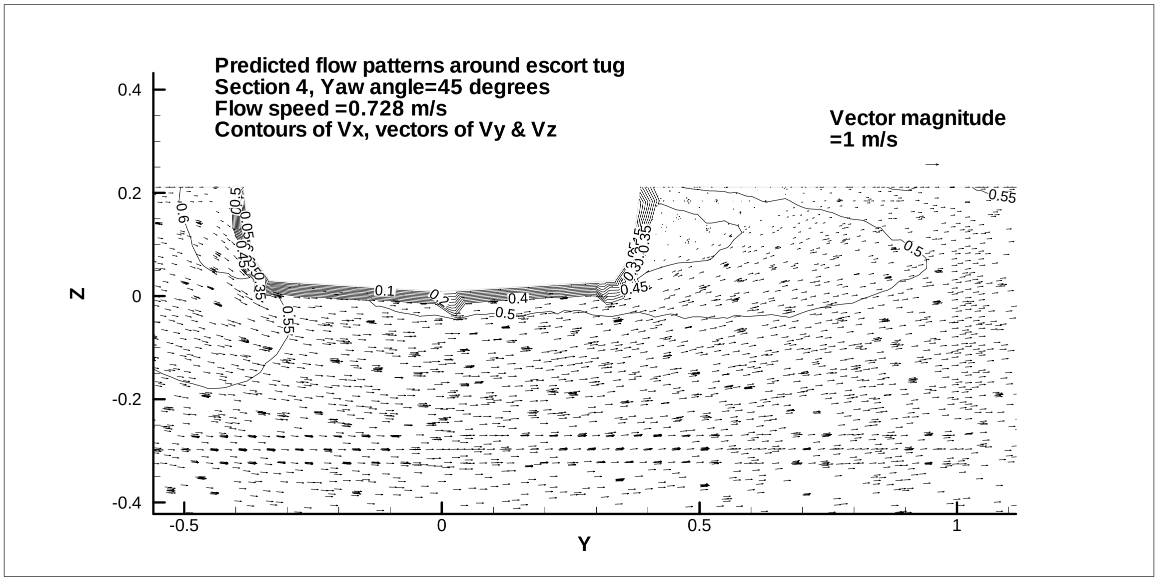

Figure 26, Yaw angle 45 degrees, without fin, section 4

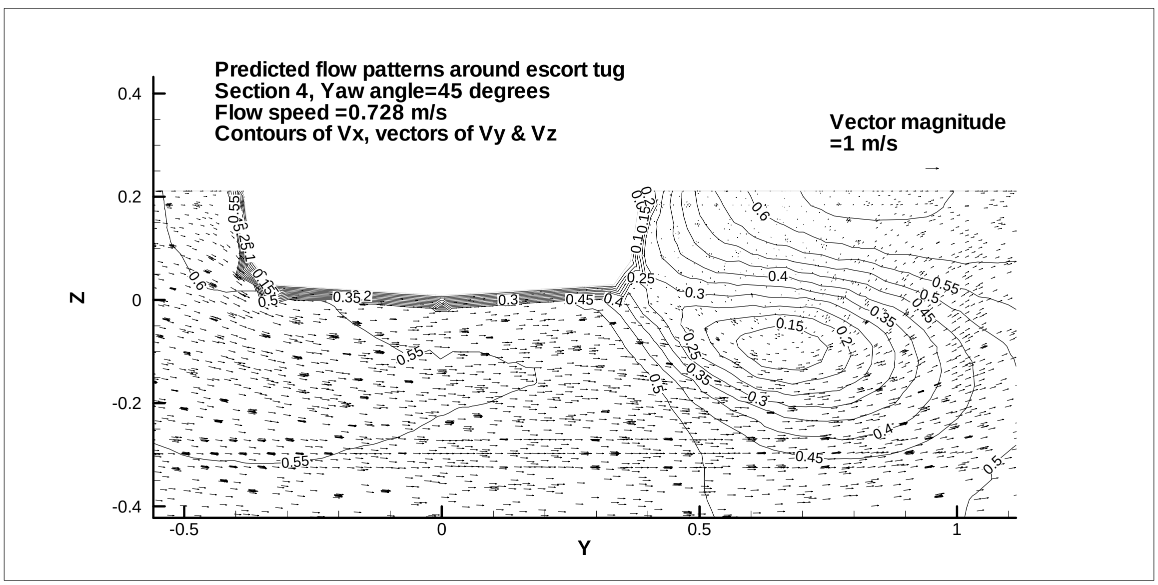

Figure 27, Yaw angle 45 degrees, with fin, section 4

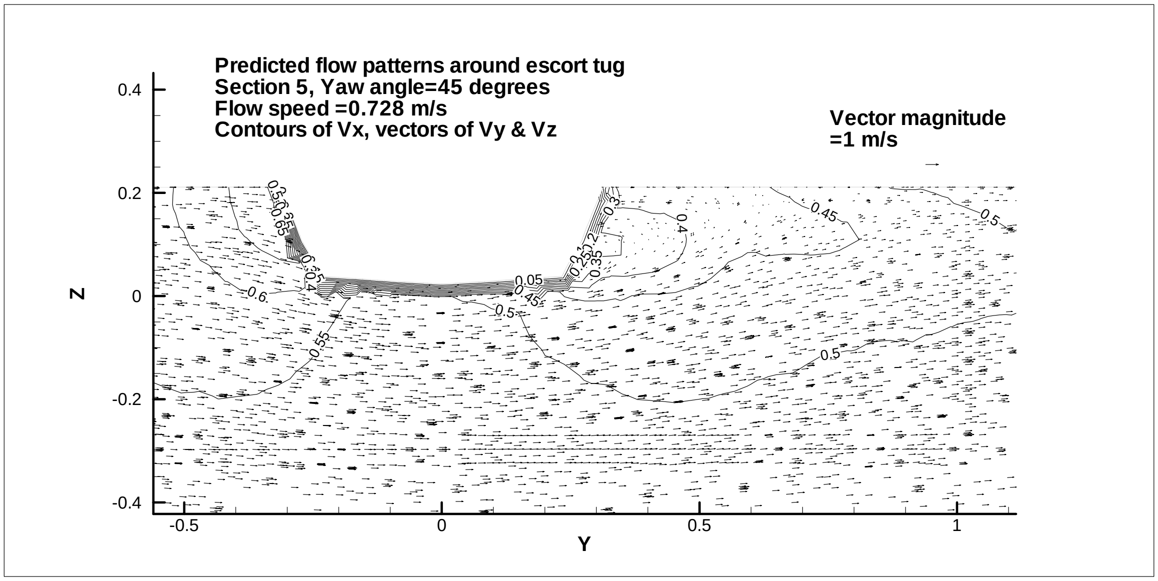

Figure 28, Yaw angle 45 degrees, without fin, section 5

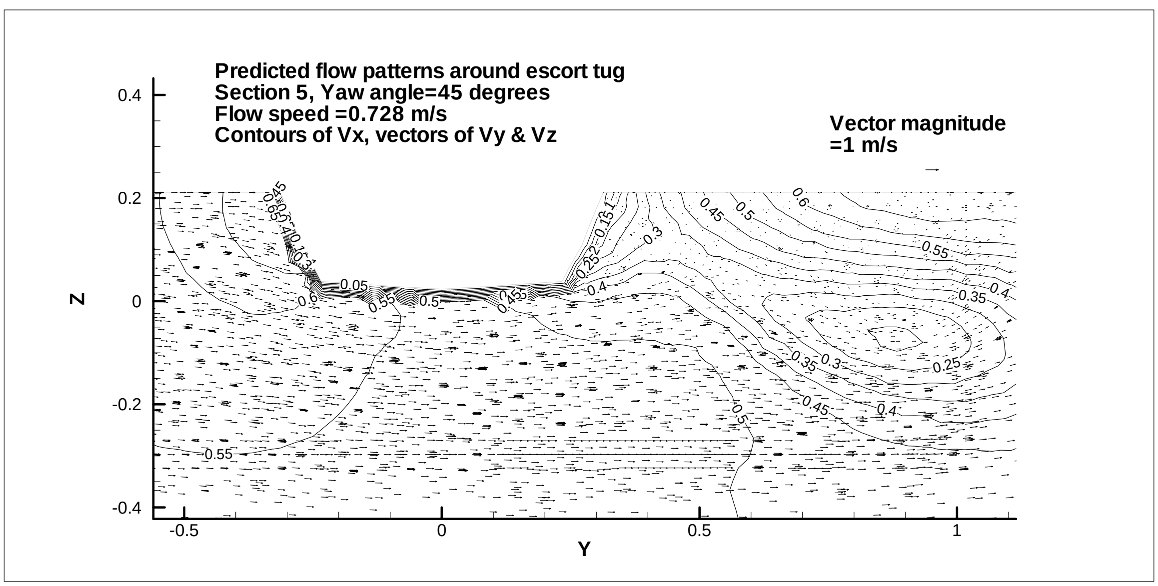

Figure 29, Yaw angle 45 degrees, with fin, section 5

DISCUSSION OF CFD PREDICTIONS OF FLOW PATTERNS

The CFD simulations described in this report have been carried out for the purpose of planning Particle Image Velocimetry (PIV) experiments to measure the flow around an escort tug. The mesh used has not been optimized or subjected to any sensitivity studies. However, comparisons between CFD predictions using *Fluent* and measured flow around scale models for a Series 60 C_B=0.6 hull for yaw angles of 10 and 35 degrees (Molyneux, 2005) showed that CFD should give predictions of the flow patterns that are accurate enough for identifying the major flow features to be investigated during the experiments.

The CFD predictions show that the presence of the fin is the dominating factor in the flow pattern (and resulting forces) around the escort tug hull. At 20 degrees of yaw, the major effect of the fin is to create a region of lower speed flow (relative to the undisturbed speed) downstream from the fin. This is seen by comparing the results of the simulations shown in Figures 30 and 31, which show three-dimensional views of velocity magnitude (defined as $(v_x^2+ v_y^2+ v_z^2)^{0.5}$) with and without the fin. For the cases with the fin, the region of lower speed flow can be seen from the contours of velocity magnitude that extend from the hull surface to approximately the maximum depth of the fin. The centre of this region of low speed flow moves from the centreline at section 1 to approximately 0.4m off the centreline, on the downstream side, at section 5. This movement is close to the angle of the undisturbed flow relative to the centreline at Section 1.

Predictions of the flow patterns with and without the fin at 45 degrees of yaw are shown in Figures 32 and 33. The effect of the fin is even more pronounced at this yaw angle. A region of very slow speed formed on the downstream side of the fin effects the flow pattern downstream, and the result is a series of closed contours under the hull with a variation in the velocity magnitude from almost the free stream speed to almost zero. The closed contours, which do not touch the hull, indicate that the fin introduces a strong rotational component to the flow at this yaw angle. The region of low speed flow under the hull acts to slow down all the flow on the downstream side of the hull, relative to the case when the fin is removed. The centre of the low speed region created by the fin moves from 0.15m off the centreline (on the downstream side) at section 1 to 0.85m off the centreline at Section 5.

When the fin is removed, for 20 degrees of yaw, the flow shows very little asymmetry in the u velocity component until section 5 (83% aft of the forward end of the waterline). This can be compared to the predictions for the Series 60 hull (Molyneux, 2005) where significant asymmetry was predicted at midships (50%L) even for 10 degrees of yaw. For a yaw angle of 45 degrees, the escort tug hull with the fin removed shows only a weak rotational flow component on the downstream side of the hull at section 4 (67% aft of the end of the waterline) whereas for the Series 60 hull, a strong rotational component to the flow was predicted at 50%L for 35 degrees of yaw. These differences are due to the significant differences in the hull shapes between the escort tug and the Series 60 hull. The escort tug is proportionally much wider (L/B=2.69) and shallower (B/T=3.74) compared to the Series 60 hull with L/B=7.5 and B/T=2.5. The flow on the downstream side of the escort tug (between the waterline and the keel) is proportionally faster than the flow on the downstream side of the Series 60 hull, while the flow over the bottom is approximately the same. As a result, there is less of a shear force gradient on the tug and a vortex will not form on the downstream side.

The fin has a relatively small effect on the upstream flow patterns at both yaw angles.

The side force measurements, shown in Figure 2 showed a peak at approximately 35 degrees, and its was speculated that this was due to the flow around the fin stalling. The CFD code can give some insight into this. Figures 34 to 36 show the calculated flow pattern in a horizontal section, taken at the mid-depth of the fin, for yaw angles of 20, 30 and 35 degrees. The vectors show in-plane velocity and the contours show velocity magnitude.

At 20 degrees, the CFD code predicts that the flow stays attached to the foil. At 30 degrees the flow has started to separate and at 35 degrees the flow shows a vortex forming on the low-pressure side of the foil. A refinement to the analysis will be to treat the hull and the fin as separate surfaces, and then the relationship between the force components can be determined.

Overall the force predictions given by the CFD code are encouraging. There is no information available on the flow patterns around this type of hull, so it is hard to discuss the results in comparison to other cases. The mesh used for these predictions was relatively crude. Some preliminary simulations run using the same mesh with an inviscid fluid showed that there was in fact very little effect of viscosity on the predicted flow patterns and forces. It is likely that the mesh for the boundary layer is too coarse, and should be refined. In most locations the boundary layer is almost entirely within the first layer of cells at the hull surface. The next level of simulation should have a finer mesh close to the hull.

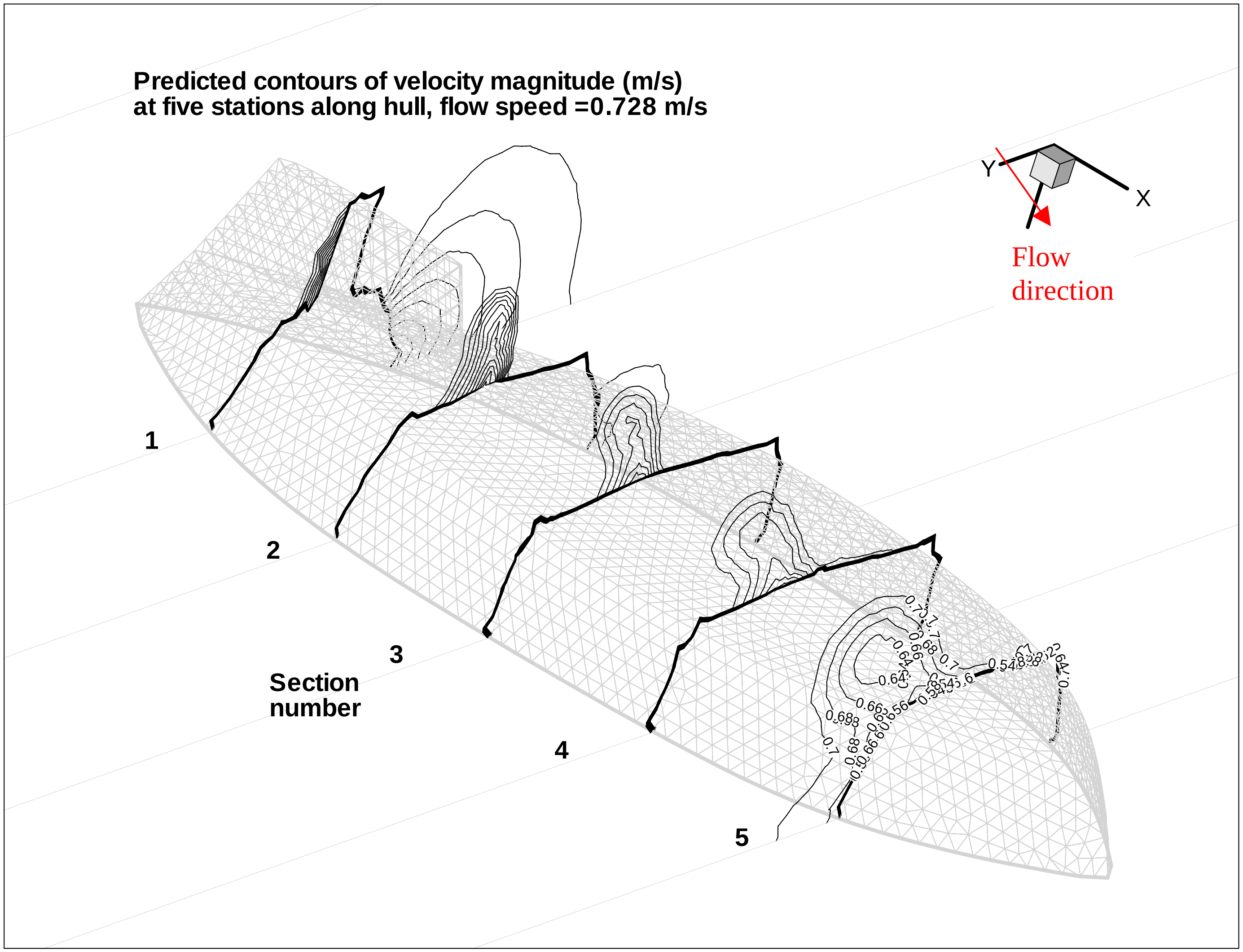

Figure 30, Contours of velocity magnitude, yaw angle=20 degrees, hull and fin

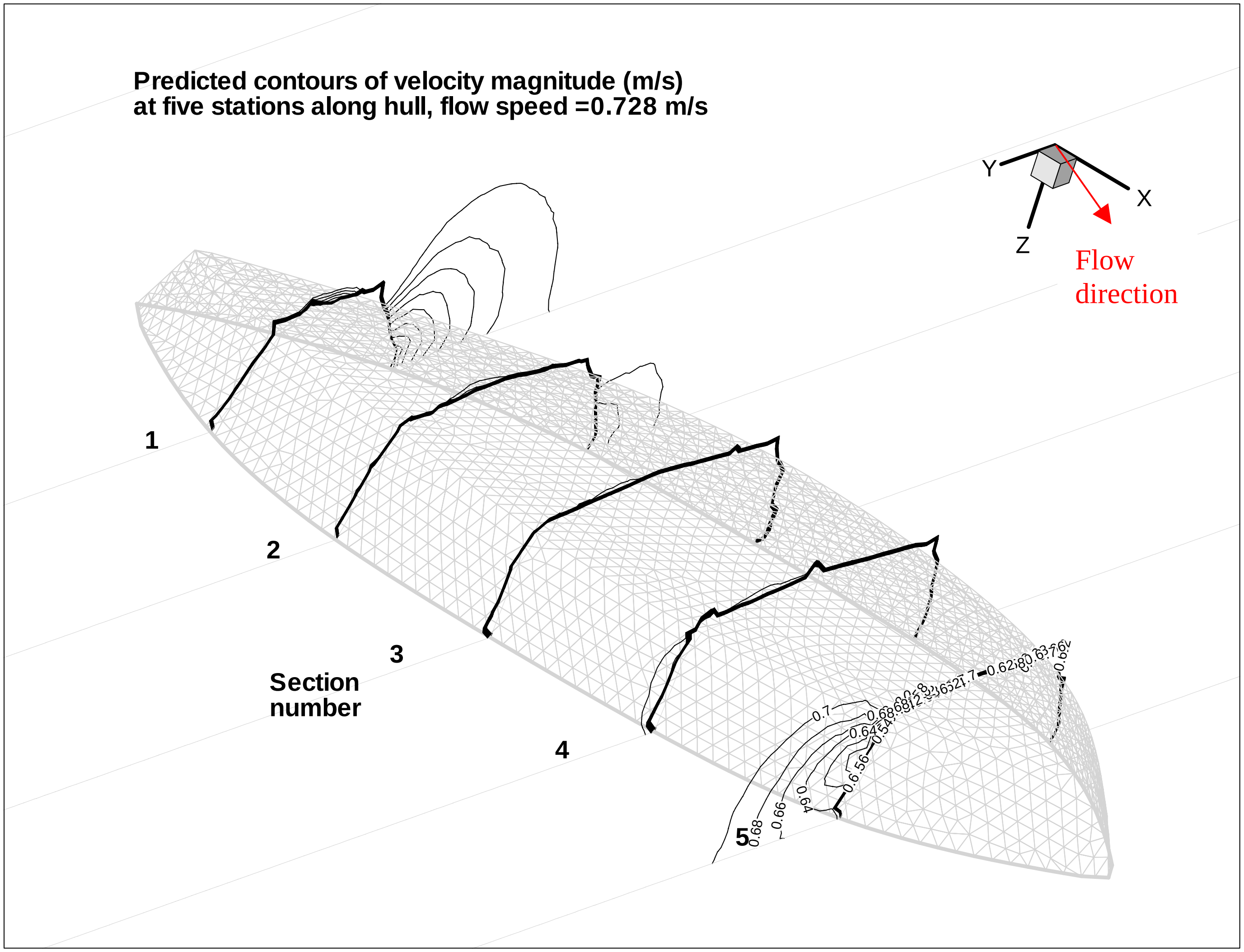

Figure 31, Contours of velocity magnitude, yaw angle=20 degrees, hull only

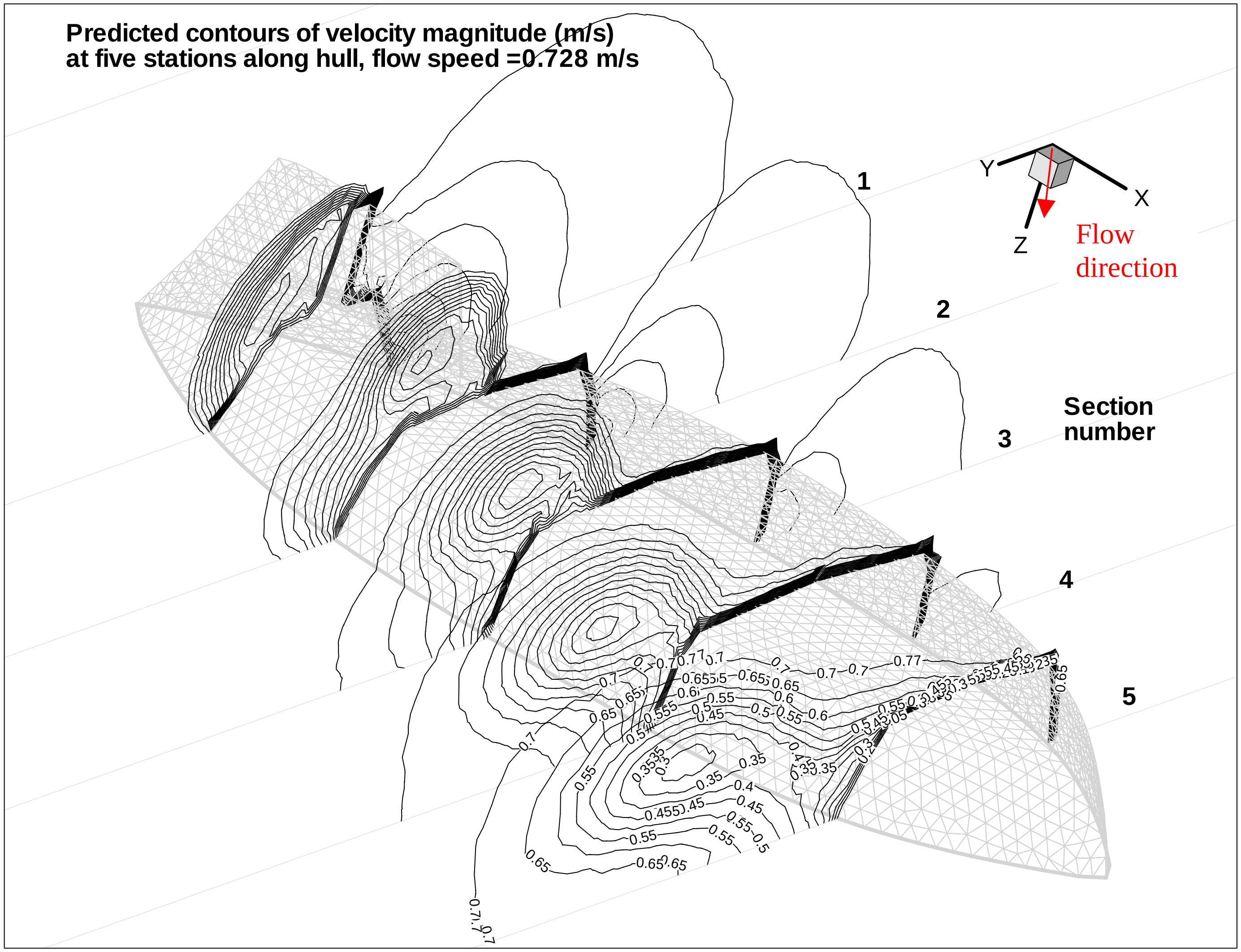

Figure 32, Contours of velocity magnitude, yaw angle=45 degrees, hull and fin

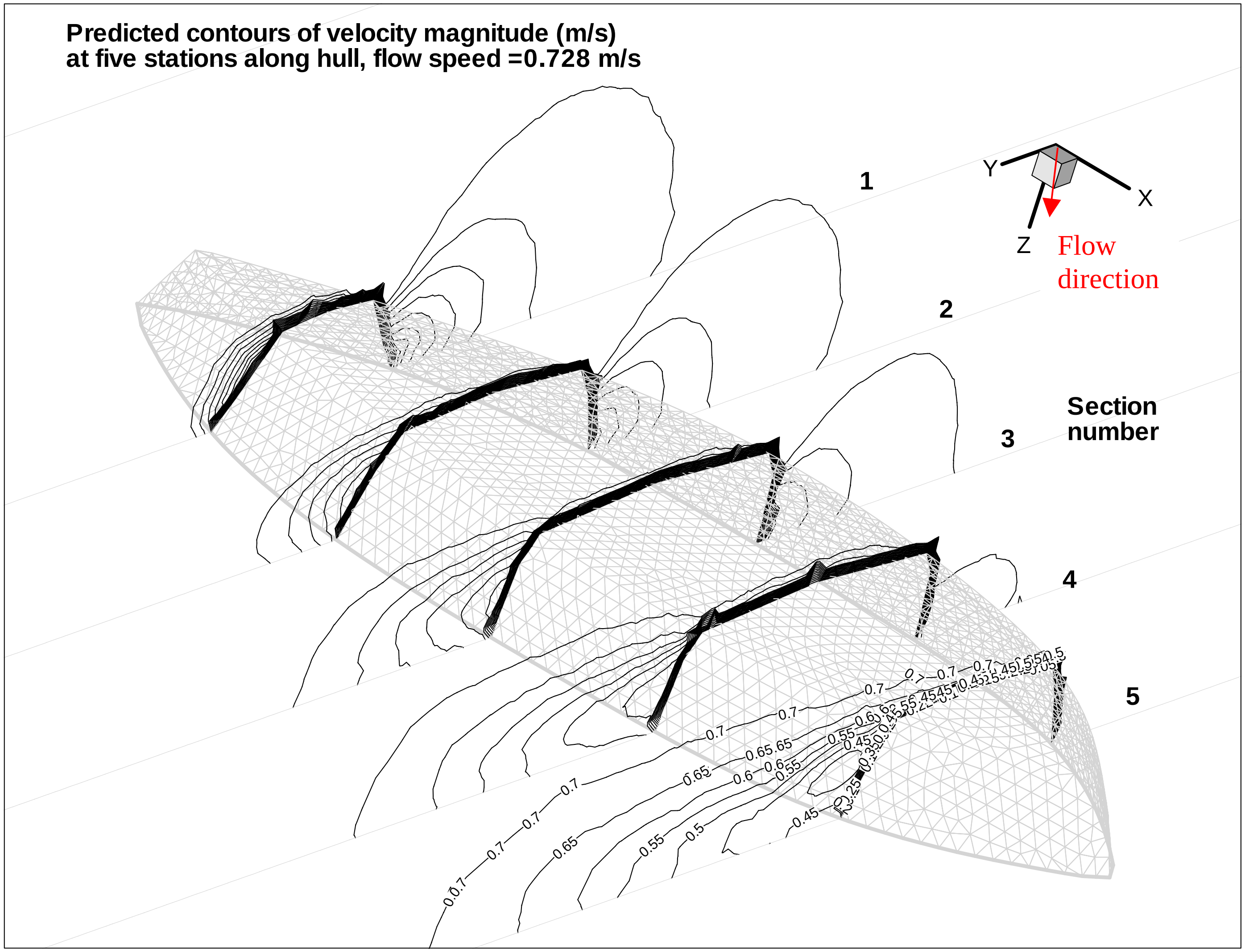

Figure 33, Contours of velocity magnitude, yaw angle=45 degrees, hull only

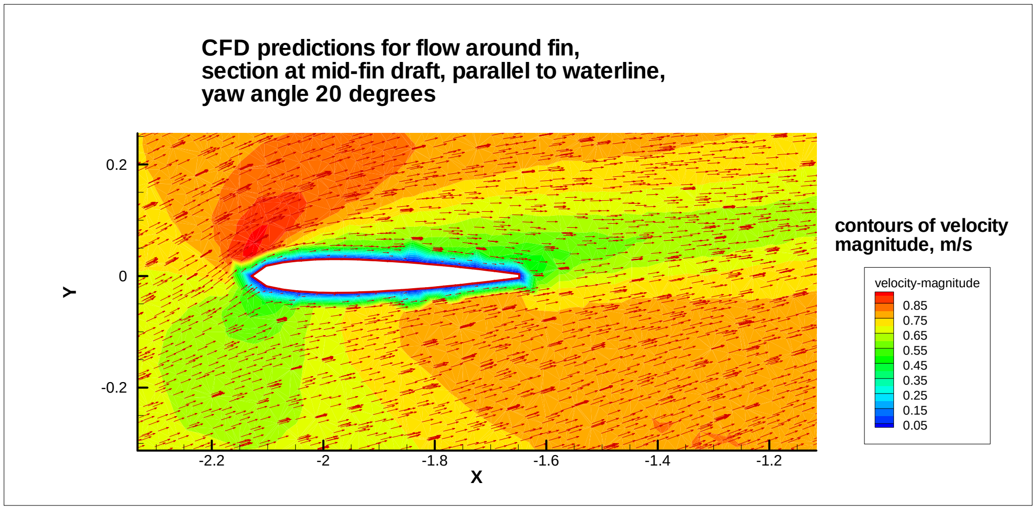

Figure 34, predicted flow around fin at 20 degrees of yaw

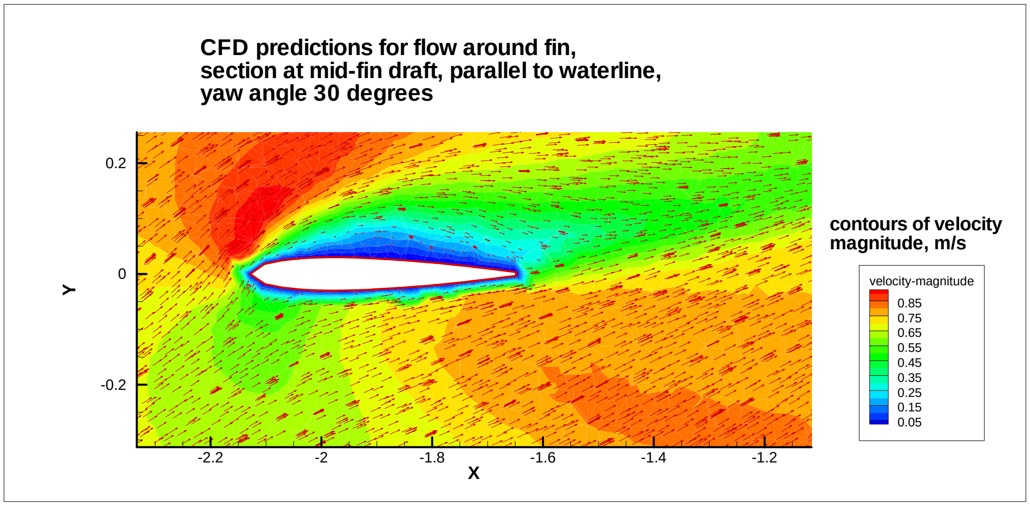

Figure 35, predicted flow around fin at 30 degrees of yaw

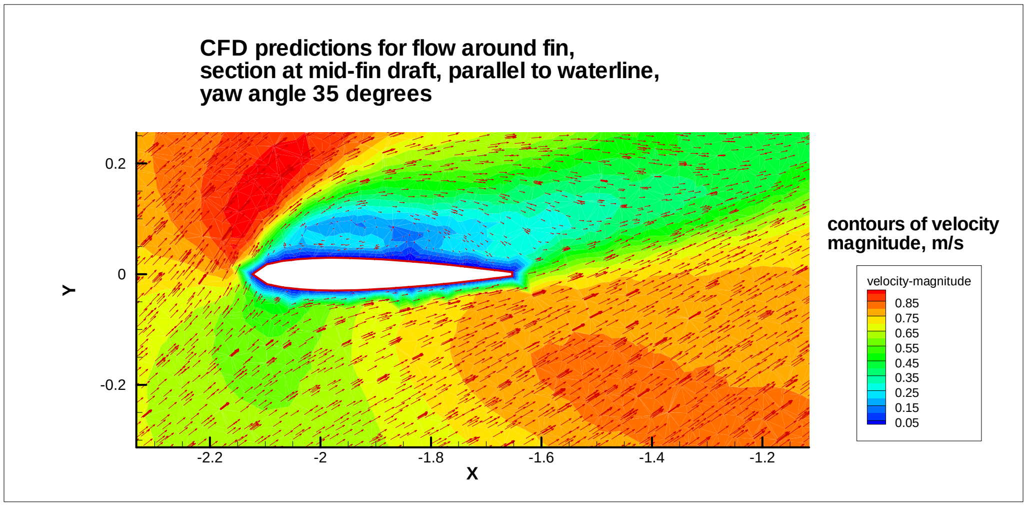

Figure 36, predicted flow around fin at 35 degrees of yaw

SUMMARY OF STEREO PIV THEORY

The essential elements of a PIV experiment are:

- A brightly illuminated plane where flow measurements are to be made within the fluid. Typically a laser is used to provide this, since the resulting light sheet is very bright with very fine tolerances for the sheet thickness.
- Seed particles within the flow, which are small (relative to the flow patterns) and neutrally buoyant. This maximizes the likelihood that the particles are following the flow patterns.
- Cameras to capture images of the seed particles. In the MUN system, these are 12 bit CCD cameras, which collect a digital image with a maximum resolution of 1376 x 1040 pixels.
- Timing devices to synchronize the light sheet and the camera shutters, so that two images of the seed particles are obtained, separated by a small time (dt).
- Software to analyze the results.

The PIV system supplied to Memorial University by LaVision Inc. (Xu et al, 2005) was designed to make collecting and analyzing flow measurements relatively straightforward, provided the user has a moderate understanding of the theory behind the methods. As with all experiment techniques there is an amount of measurement uncertainty within the system. In this section, the basics of PIV measurement and analysis techniques (as implemented within the LaVision software packages) are reviewed and the implications on the level of measurement uncertainty are discussed.

The software supplied with the system was FlowMaster, a specialized computer code for data acquisition and analysis in PIV and PTV experiments (LaVision GmbH, 2002). FlowMaster is a subset of a generalized image processing and analysis software package (DaVis, LaVision GmbH, 2003), adapted to automate many of the routine requirements of PIV experiments.

The fundamental assumption in PIV analysis is that the calculated flow vectors follow a linear path based on the average seed particle displacement within a small area of the flow pattern being studied. If there is a high degree of curvature to the flow, relative to the size of the interrogation window, the calculated particle traces will not match the real flow conditions. PIV will be most accurate for small interrogation windows and will be inaccurate for flow conditions where circulation occurs within an interrogation window. The size of the interrogation window must be decided a priori or by trial and error. If trial and error is used, the interrogation window sizes used in the analysis are reduced until there is no significant change in the calculated flow patterns.

The basis data product from each CCD camera is a pair of images of particles within the flow, separated by a time interval, dt. Each image represents a 2-dimensional projection of the seed particles within the illuminated plane. The first step is to analyze each image pair in the image plane of the camera. The total CCD image is divided into square interrogation windows (i.e. 128 x 128 pixels). A cross-correlation procedure is carried out to determine the correlation between pixel images in the first frame and the second frame.

The correlation function for one camera is of the form:

$$C(dx, dy) = \sum_{x=0, y=0}^{x<n, y<n} I_1(x, y) I_2(x + dx, y + dy), \frac{-n}{2} < dx, dy < \frac{n}{2}$$

I_1 and I_2 are the image intensities (grey scale) of the first and second interrogation windows, and the 2-dimensional array C gives the correlation strength for all integer pixel displacements (dx, dy) between the two interrogation windows. The size of the window is n x n pixels. This is also usually the size of the correlation plane, so that the maximum displacement calculated is $\pm$n/2. If a single pass analysis procedure is used, the interrogation windows have the same pixel coordinates in each frame.

The peak of the correlation function gives the most likely mean value of particle movement within the interrogation window (dx,dy). The position of the correlation peak can be identified to sub-pixel accuracy and the expected accuracy is between 0.1 to 0.5 pixels (LaVision GmbH, 2002). Individual peaks are determined from a three point Gaussian function. The actual resolution depends on the image quality, which is influenced by particle size, particle density and contrast.

The correlation procedure is repeated for each interrogation window and for each camera, resulting in two sets of vectors (Vx_1, Vy_1) for camera 1 and (Vx_2, Vy_2) for camera 2. The required vector is (Vx, Vy, Vz) relative to the plane of the light sheet. The set of equations determined from the two cameras is over specified in that there are four variables available to solve for three unknown quantities. This feature can be used to improve the accuracy of the PIV measurement by providing an additional check on vector accuracy. The linear equation system is solved by the normal equation and the remained degree of freedom error should be small (>3 pixels), which provides a criterion for removing spurious vectors.

A problem that occurs when a camera is recording an image from an oblique plane is that the depth of field of the lens becomes reduced and the image is only in focus at the centre of the lens. This can be corrected by using the Scheimpflug criterion, which requires the object plane, the image plane and the plane of the lens to intersect on a common axis. In practical application, the lens is rotated relative to the image plane, which requires a special adapter fitted to the camera. The result is a constant depth of field over the image, but increased perspective distortion.

Image distortion correction is an essential part of stereo PIV analysis because the image plane of the two cameras will always be at an angle to the object plane. In order to correct for the distortion between the two images a calibration procedure is carried out. For stereoscopic PIV this requires two planes with marks at known locations on a grid that covers the complete field of view of each camera.

The mapping function used for image distortion correction in the DaVis FlowMaster software is a third order two-dimensional polynomial function to map x_1 and y_1 in pixel coordinates within the image plane for camera 1 (including distortion) to corrected coordinates x and y in the object plane without distortion. The mapping function (for camera one at on z location) is of the form:

$$\begin{pmatrix} x_1 \\ y_1 \end{pmatrix} = \vec{f}\begin{pmatrix} x \\ y \end{pmatrix} = \begin{pmatrix} x + dx_1(x, y) \\ y + dy_1(x, y) \end{pmatrix}$$

With the normalized coordinates

$$s = \frac{2(x - x_0)}{nx}$$

$$t = \frac{2(y - y_0)}{ny}$$

defined by image size nx, ny (in pixels) with the origin (x_0, y_0) at the midpoint of the image. The values of dx_1 and dy_1 are given by

$$\begin{pmatrix} dx_1 \\ dy_1 \end{pmatrix} = \begin{pmatrix} a_0 + a_1 s + a_2 s^2 + a_3 s^3 + a_4 t + a_5 t^2 + a_6 t^3 + a_7 st + a_8 s^2 t + a_9 st^2 \\ b_0 + b_1 s + b_2 s^2 + b_3 s^3 + b_4 t + b_5 t^2 + b_6 t^3 + b_7 st + b_8 s^2 t + b_9 st^2 \end{pmatrix}$$

An additional set of coefficients is obtained for camera 1 at the second z location and two sets of coefficients for camera two at the same two z locations as camera 1, for a total of four mapping functions. The calculation of the mapping functions requires at least 40 common grid points being visible in both camera images. For stereo PIV, the image distortion correction is applied to the vectors for each camera, calculated using the correlation function, rather than to the particle images.

The mapping functions are determined empirically using stereo images of a specially manufactured plate. The plate is machined so that each face is stepped with two parallel planes. Each plane has a matrix of white markers, evenly spaced at 22.5 mm. The step between the faces of the plate is 9 mm. The advantage of this approach is that two parallel planes are accurately defined relative to each other. It is critically important that the calibration plate is located within the laser sheet and parallel to it, even though the calibration is carried out using visible light. Any rotation between the laser and the calibration plate will reduce the accuracy, since the vectors will be calculated in the reference frame of the calibration plate, not the frame of the light sheet.

For the analysis of the mapping function, the DaVis software calculates the size of the average deviation between the calculated position of the marks and the actual positions. The software manual (LaVision GmbH, 2002) states that a good calibration is considered to have an average error in the mapping function of less than 0.5 pixels and recommends that experiments should not be carried out if the average deviation is more than 2.0 pixels. The dialogue box also gives the dimensions of the 3-D image (in pixels), a chi squared statistic for the x and y directions, the number of marks used for calculating the mapping function and the average peak ratio (intensity) of the marks. The calibration procedure reduces the area of the object plane to the area common to both cameras. The size of the image common to both cameras is greatest when the reference point is at the same pixel coordinate in both views, and the cameras are symmetrically located about the image plane.

The basic image analysis procedure described above can be refined to increase the signal to noise ratio. Initially, the division of the pixel image of the seed particles into interrogation windows was based on the geometry of the window and not the flow pattern. Particles close to the downstream edge of an interrogation window at the first exposure may have moved out of that window in the second exposure, and new particles will have flowed in. As a result, the number of particles common to both views is reduced.

Using one of the following techniques can increase the number of particles included in the analysis:

- Overlap windows: The second interrogation window includes an overlap with neighbouring windows, based on a fixed fraction of the original grid.

- Adaptive Multiple passes
    - Fixed window size: Uses vectors calculated in first iteration to move the second interrogation window off the initial grid.

    - Reduced window size: For the second iteration, the window size is half the initial size, and the shift relative to the original window is calculated based on the mean vector calculated in the first pass.

The origin for starting the analysis of the PIV images is the top left corner of the CCD image. If a fixed window size is used, there may be parts of the image that are not processed (bottom and right side) if the full image dimension is not an integer number of interrogation windows.

Once the flow vectors have been computed for an equidistant grid, further processing can be carried out to improve the quality of the image by removing spurious vectors. These include:

1. Allowable vector range
The calculated vectors are filtered on the basis of allowable ranges (in pixel or m/s). The range is specified based on a mean value, with upper and lower limits (which are the same).

2. Peak ratio

The peak ratio factor Q, compares the magnitudes of the highest peak in the correlation coefficient matrix relative to the noise and the second highest peak relative to the noise, based on the function

$$Q = \frac{P_1 - \min}{P_2 - \min}$$

where P_1 is the highest value in the correlation matrix, P_1 is the second highest peak, and min is the lowest value. For Q=1.5 or higher, the main peak is well defined and probably represents a valid vector. Peak ratios close to 1.0 most likely represent invalid vectors and should be removed.

3. Median filter

In this case, the analysis is based on a three by three grid of interrogation windows, and the vector in the centre square is compared to the values in the other eight squares. The centre vector is rejected if it is outside the range given by the median vector of the eight neighbours, plus or minus a deviation based on a multiple of the rms of the neighbouring vectors. Another criterion for filtering includes removing the vector if there are less than a set number of neighbouring cells with calculated vectors.

In some cases, the background to the particle image may not be a constant intensity. This is most likely to occur in regions of the image close to the solid boundary of a model, where the laser light is reflected. To improve particle images in these situations, a filter, similar to a high pass filter, can be used. The aim is to make the background more uniform and increase the contrast between the particles and the background. To obtain this condition, a scale parameter is used, which must be at least twice the mean particle diameter in pixels. An alternative is to subtract a constant value. The disadvantage of this technique is that some information is being removed from the image, and the user must be sure that the information being removed is less important than the information being retained.

Successfully seeding the flow is a key factor to obtaining reliable results from PIV experiments. The seed particles should be neutrally buoyant in the test fluid, so that there are no velocity components occurring due to gravity or buoyancy forces. Also, the particles should be small in relation to the flow patterns, so that the particles follow the local movement of the fluid, not the motion due to average fluid forces acting on the particle. Experiments carried out so far at Memorial (Xu et al, 2005) have used silver coated hollow glass spheres, with an average diameter of 14 μm and a density of 1.7 g/cc.

The advantage of the silver coating is that it is highly reflective to laser light and the particles appear bigger than actual size when viewed in the CCD camera. It is desirable to have particle diameters viewed at the CCD between two and three pixels. The DaVis software uses a three-point Gaussian peak approximation on the measured intensities to identify the centre of a seed particle to sub-pixel accuracy. If the image size is less than one pixel, there is a tendency for the calculated vectors to be integer numbers of pixels and resolution of the vector field is compromised.

The accuracy of the vector calculation within a given interrogation window increases with the number of particle image pairs included in the correlation calculation. In practice three or four particle image pairs in each interrogation window are sufficient for accurate definition of the correlation peak. Increasing seed density means that the size of the interrogation window can be reduced, with the result that the spatial resolution of the flow can be increased. The upper limit of seeding concentration is that there must be a clear contrast between particles and the background

Particles are excluded from the calculation if they flow out of the measurement space of either camera during the time interval dt. The particles can move out of the in-plane interrogation window, or if the flow is three-dimensional, they can flow out through the plane of the light sheet. The value of dt to minimize the loss of seed particles from within the laser sheet depends on the local flow velocity components for the experiment and must be adjusted accordingly. The reliability of vector calculations will be increased considerably by aligning the laser so that the weakest flow component is through the plane of the laser. .

The final factor to consider in determining the accuracy of PIV measurements is the number of images of the same nominal flow condition. The accuracy of steady flow conditions can be improved if the vectors are based on the average value from multiple image pairs. The number of frames used to determine this will depend on factors such as the degree of spatial resolution required and the length of time available for the experiment.

PREVIOUS APPROACHES TO ESTIMATING UNCERTAINTY IN STEREO-SCOPIC PIV EXPERIMENTS

Uncertainty in stereoscopic PIV systems has been studied in the literature. The theoretical errors in the vector reconstruction from stereo images have been determined (Lawson and Wu, 1997). The uncertainty in translational systems (with no Scheimpflug correction) and rotational systems (with Scheimpflug correction) were determined. The focus of the analysis was on determining the relative error between the in-plane vectors (x, y) and the through plane vectors (z) and results were presented in the form of an error ratio, rather than an absolute value. The objective was to determine the arrangement of the PIV system with the minimum uncertainty in the z direction, relative to the x-y plane.

To carry out this analysis it was assumed that the uncertainty in the vectors determined at the object plane (x, y, z) was represented by an RMS value and that this value was equal in each direction. Then, by considering the geometry (distances between cameras and viewing angles) and the magnification of the PIV system, the error ratio (uncertainty) based on the geometric reconstruction was calculated. The error ratio can be mapped over the complete object plane.

The analysis showed that at the centre of the lens, the two systems produced very similar ratios, but as the distance off the centre was increased, the error ratios for the rotational system were up to 40% lower than the for the translational system. This analysis did not consider any errors due to distortion correction.

The same authors carried out an uncertainty analysis of a complete stereoscopic PIV system in another paper (Lawson and Wu, 1997). This was an experimental approach to uncertainty analysis, starting with determination of the 3-D mapping function, using a plate similar to the one provided to Memorial University.

A test PIV specimen was constructed by suspending seed particles in epoxy resin. The advantage of this approach was that it used real seed particles, but fixed them relative to each other. When the block was moved all particles were moved a constant distance and the resulting vectors calculated by the PIV software should be constant across the whole field of view for each camera. The test specimens were illuminated using laser light, and images collected. The specimen was then moved known distances (δx, δy, δz) and the distances calculated by the PIV system were compared to the known distances. Different viewing angles between 10 and 45 degrees were evaluated, but the cameras were always on the same side of the light sheet, and at the same viewing angle relative to the light sheet.

The authors conclude that optimum performance will be obtained by using viewing angles between 20 and 30 degrees for camera *f* numbers of *f*16 and higher. The uncertainty analysis for uniform flow gives rms errors of 1-2% for the in-plane flows and 3-4% for the through plane flow (which was within the range of 8% to 18% of the theoretical error). These values were for cases where particle movement was restricted to between 15% and 30% of the interrogation window dimension. Below this displacement range, the system did not have enough resolution.

Other researchers have used variations on the basic approach taken by Lawson and Wu. Soloff et al (1997) investigated the robustness of a 3-dimensional mapping function for stereoscopic PIV analysis. They used an aluminium calibration plate with a 9 by 9 grid of holes, 0.5mm diameter at 27mm intervals. The plate was lit from behind. The calibration procedure was to take images of the plate at three z locations of 0, +/-0.5 +/-0.005mm. This gave rms errors in the mapping function of 1.1 pixel for camera 1 and 1.2 pixel for camera 2. This translated to 0.045mm and 0.051 mm respectively.

After the calibration, images of the plate were taken with each camera, and then the plate was moved small but known distances in y and z directions, and images of the plate at the new location were taken. Cross correlation was used to analyze the image pairs from each camera. The two-dimensional vector fields for each camera were filtered and then stereoscopically combined to obtain the three-dimensional vectors (x, y, z) calculated from the PIV software.

The errors between the calculated vectors and the known movement of the calibration plate (in each direction) were plotted as contours of error against the x and y coordinates for the measurement space. The results were contours of error, spatially distributed over the measurement area.

The estimated error (based on the highest contour shown, which looks to be about 95% of all measurements) for each axis was

x +/-0.0050 mm
y +/-0.0036 mm
z +/-0.0200 mm

Resulting errors were not evenly distributed over the measurement space, and it would have been useful to see an overall statistical distribution of the errors. The error in the results was the same order of magnitude as the error calculated from the mapping function for each camera during the calibration, so in this case the mapping function is the primary source of the error.

Calcagno et al. (2002) discussed the uncertainty of a stereoscopic PIV system designed for ship model testing in a cavitation tunnel to measure flow in the wake of a propeller. An underwater camera was aligned directly behind model to measure flow in the plane of the propeller. The second camera, mounted outside the cavitation tunnel had a viewing angle between 36 and 40 degrees off the centreline of the model.

For the camera looking directly at the in-plane vectors, the mapping function had an estimated particle resolution within 0.1 pixels (4 cm/s for the flow conditions considered). This view was treated as a two dimensional view, with minimal distortion. Error in the through plane measurements was thought to come from the stereo reconstruction (mapping function). This was analyzed using a target consisting of a ‘typical’ PIV image, which was moved a known distance (1mm) along the normal axis. The calculated uncertainties were under 2.5% in the ‘in-plane’ displacements and under 3% in the through plane displacements. The authors discuss the fact that the errors may be optimistic, since they were obtained from a bench test, without the model, the rotating propeller and the light reflections that they cause were omitted.

RECOMMENDED PROCEDURES FOR ESTABLISHING UNCERTAINTY OF PIV SYSTEM AT MEMORIAL UNIVERSITY

The major source of uncertainty in stereoscopic PIV analysis is likely to come from the mapping function for correcting image distortion and the peak identification for individual particles. Based on a preliminary review of the literature, the most appropriate determination of uncertainty for practical flow measurements will be a determination of the uncertainty of the total system performance. The most feasible way to determine these values will be a special set of experiments using Memorial University's PIV system. Since the vast majority of flow measurements will be carried out in water, the uncertainty experiments should be carried out in one of the small tanks with a stationary PIV system, rather than in the OERC towing tank.

The PIV system should be set up in its typical operating condition, and calibrated using the manufacturers recommended procedure. Prior to this, a test image should be made. Although the approach taken by Lawson and Wu is very attractive, since real seed particles are used, learning the required techniques for construction might be very time consuming. As a result, the recommended approach is to make a target plate (similar to that used by Soloff et al), with a grid of very small holes. This will be placed underwater, within the plane of the laser, on a micrometer table (or some similar device) that will allow precise movement of the plate.

Stereoscopic images of the target plate will be collected using the CCD cameras for a range of movement within the laser sheet (δx, δy, δz) and the resulting errors mapped over the image space. If necessary, the procedure will be repeated for the range of PIV system arrangements typical of the expected conditions for Memorial University's facilities. This should give a practical estimate of the uncertainty in the measurement system, and mean that the uncertainty will only have to be re-determined if there is a major change in the set-up of the PIV system for a particular experiment program.

In addition to the establishment of actual levels of uncertainty, the theoretical values can be determined using the approach of Lawson and Wu (1997).

PARTICLE IMAGE VELOCIMETRY EXPERIMENTS TEST PLAN

Experiments to determine the hydrodynamic forces on an escort tug hull form showed that the fin generates up to 50% of the total load (Molyneux, 2002). The preliminary CFD simulations described in this report showed good agreement with the force measurements and that the fin creates a region of slow moving flow under the hull. The difference in flow patterns between the cases with and without fin should be confirmed with experimental data.

A yaw angle of 20 degrees was the approximate limit for good agreement between forces predicted by the preliminary CFD simulations and experiments. A yaw angle of 45 degrees is the mean operating yaw angle for a tug in escort mode. Using Froude scaling, 0.5 and 1.0 m/s for the model correspond to speeds of 4.1 and 8.2 knots for the ship (at 1:18 scale). These represent typical speeds within the operating range of a tug, which is normally from 4 to 10 knots.

A summary of the proposed test plan is given in Table 5.

Model speed, m/s	Yaw angle, deg.	Fin
0.5	20	Yes
0.5	20	No
1.0	20	Yes
1.0	20	No
0.5	45	Yes
0.5	45	No
1.0	45	Yes
1.0	45	No

Table 5, Overview of test plan

If flow patterns at these speeds or yaw angles prove to be too difficult to measure for any reason, yaw angles of 10 degrees and 35 degrees (the same ones used for the Series 60 C_B=0.6 model) would the second choice. Comparing the escort tug results with the Series 60 results will give information on the effect of hull shape on flow patterns at high yaw angles. A further simplification will be to reduce the test speeds (e.g. 0.25 and 0.5 m/s).

The preliminary CFD simulations indicate that when the fin is fitted, there will be a vortex in the flow, which starts at the fin and moves downstream with the flow. The preliminary PIV experiments (Molyneux and Xu, 2005) showed some circulation in the flow at a section close to midships, on the downstream side of the hull. The circulation and vortex core were clearly visible when the laser plane was oriented across the tank. Given these observations, the most useful results should be obtained with the laser in this orientation. Measurements will be made at several locations along the hull on the upstream and downstream side of the hull, with and without the fin in place. In order to track the movement of the vortex, between three and five longitudinal locations along the hull are required.

Measurements in the orthogonal plane (parallel to direction of motion) will also be useful for CFD validation and checking the functionality of the PIV system, although the flow patterns are likely to be less distinct. Experiments will be carried out for at least one measurement plane (intersecting the model at midships) on the downstream side of the hull only.

It will be possible to remove the fin with the model in the water, and so the PIV system will not need to be moved. This will ensure that the spatial location of the measurement area, relative to the model, will be the same for the cases with and without a fin at each location.

Based on the CFD predictions for 45 degree yaw angle, the measurement area for each section should cover at least the range of dimensions given in Table 6. These may be adjusted depending on the actual flow conditions or the constraints imposed on the movement of the PIV system by the carriage geometry. The maximum value for the downstream side can be reduced for 20 degrees of yaw.

Section	X/Lwl (at hull)	Y range, m, No fin,	Y range, m, With fin	Z range, m, No fin,	Z range, m, With fin,
1, D	0.832	0.0 to 0.5	0.0 to 0.6	-0.1 to 0.2	-0.3 to 0.2
1, U	0.832	-0.5 to 0.0	-0.5 to 0.0	-0.1 to 0.2	-0.3 to 0.2
2, D	0.666	0.0 to 0.6	0.0 to 0.7	-0.1 to 0.2	-0.3 to 0.2
2, U	0.666	-0.5 to 0.0	-0.5 to 0.0	-0.1 to 0.2	-0.3 to 0.2
3, D	0.500	0.0 to 0.8	0.0 to 1.0	-0.1 to 0.2	-0.3 to 0.2
3,U	0.500	-0.5 to 0.0	-0.5 to 0.0	-0.1 to 0.2	-0.3 to 0.2
4, D	0.334	0.0 to 0.8	0.0 to 1.0	-0.1 to 0.2	-0.3 to 0.2
4, U	0.334	-0.5 to 0.0	-0.5 to 0.0	-0.1 to 0.2	-0.3 to 0.2
5, D	0.168	0.0 to 1.0	0.0 to 1.3	-0.1 to 0.2	-0.3 to 0.2
5, U	0.168	-0.5 to 0.0	-0.5 to 0.0	-0.1 to 0.2	-0.3 to 0.2

Table 6, Estimated measurement ranges, yaw angle 45 degrees,
D=downstream side of hull
U=Upstream side of hull

The dimensions given in Table 6 are for the hull based coordinate system used for the CFD simulations and shown in Figures 10 to 33. The PIV system will be set up in a tank based coordinate system (with orthogonal axes in directions parallel to carriage motion, perpendicular to carriage motion and vertical). The proposed origin for the coordinate system used for the experiments will be the intersection of the waterline and forward end of the centreline of the hull.

The measurement planes in the tank-based system will not be at constant grid locations within the hull-based system. Also, the upstream and downstream measurement planes will not be normal to the centreline of the hull. For the downstream side the measurement plane will intersect the centreline at less than 90 degrees and the upstream side will intersect at more than 90 degrees. This was accepted since the maximum range of the PIV system will be obtained when it is mounted on the west side of the carriage and the yaw angle adjustment for the yaw table is not symmetric. As a result, it only turns in one direction. The direction of motion for the model will be reversed to obtain upstream and downstream measurements. Measurements of flow on the downstream side will be made with the model moving towards the wave maker, and on the upstream side with the model moving towards the beach. The model and yaw table will be reversed within the test frame to obtain flow measurements on the downstream side.

The same coordinate system will be used for model experiments and CFD simulations. The results of the final CFD simulations (including the walls and bottom of the towing tank) will be interpolated at the same locations as the measurement planes, and the flow speeds measured during the PIV experiments will be compared directly with the results of CFD simulations.

PREVIOUS EXPERIENCE

Some preliminary Particle Image Velocimetry (PIV) experiments (Molyneux and Xu, 2005) showed that it was possible to obtain flow patterns around an escort tug model at yaw angles of 25 degrees and 45 degrees for a carriage speed of 0.5 m/s. This experience will form the basis of the plan for the experiments proposed in this report.
The major limitations of the previous experiments were that:

- The model was in the wrong orientation (fin aft not fin forward).
- The measurement region at 45 degrees yaw was too small, relative to the flow patterns (only one section was measured, and the seed density over the whole area was not consistent).
- The location of the measurement area relative to the model was not well defined.

The results of the preliminary experiments for a speed of 0.5 m/s showed that the flow patterns measured using PIV appeared to be small variations in magnitude and direction about a mean value, when averaged over 50 individual frame sets, representing approximately 20 seconds of data collection. It is possible that at 1.0 m/s the flow will become more turbulent, and as a result the test plan may have to be modified.

Another possibility is that seeding the flow at 1.0 m/s will be more challenging than at 0.5 m/s, since seeding particles disperse much more quickly as the flow speed increases. Based on the CFD predictions, the important flow features are expected to occur under the hull, and this should make seeding relatively easy, since the hull does not block the flow. The preliminary experiments showed that the biggest problems in seeding the flow occurred on the downstream side of the hull close to the waterline. Measurement areas extending below the hull could be successfully seeded upstream of the model. For these experiments it is proposed to start with the same seeding system as that used in the first round of experiments. Some small modifications will be made such as a smaller diameter tube or a faired tube to reduce the wake, and closer discharge hole spacing to increase the seeding particle density. The seeding system may need to be adapted as the experiments progress.

The preliminary experiments were carried out for two orientations of the laser plane. The first set of data was obtained for the laser parallel to the direction of motion of the carriage, and the second set was obtained with the laser perpendicular to the carriage motion. In either of these orientations, it was very easy to adjust the vertical depth of the measurement plane by raising or lowering the laser and borescope units on the mounting frame. When the laser was directed normal to the direction of carriage motion, longitudinal adjustment of the measurement plane relative to the model was possible by moving the laser and the borescopes along the mounting frame, but taking care to keep the relative spacing the same. This was necessary to avoid recalibrating the system for each field of view. The same approach could be used for movement of the measurement plane in the transverse direction, but this was more difficult since the test frame caused more restriction to movement of the PIV system components.

Given the restrictions placed on the movement of the PIV system by the carriage geometry and the relatively large size of the model, it may not be possible to obtain flow measurements at all locations within the range discussed above. In addition, variation in seeding concentration within a frame will also reduce the effective measurement area. The effect of these uncertainties can be reduced by ensuring that there is at least a 50% overlap of the viewing area between measurement frames. This should be the actual viewing area, including seeding particles, rather than the nominal area based on spatial geometry.

For preliminary experiments, the measurement area did not extend under the hull. The calibration plate was held close to the model and the PIV system was adjusted to obtain the correct viewing angle. For the experiments proposed here, it is necessary to measure flow patterns well under the bottom of the model. In this case it will be necessary to support the calibration plate under the hull. A cantilever frame has been built for this purpose. This frame can move longitudinally for different measurement sections, and can be adjusted vertically and transversely.

The size of the measurement ‘window’ for the PIV system, typically 200 mm by 200 mm is relatively small in relation to the flow structures created by a 1:18 scale model of an escort tug. This size difference requires that the ‘window’ be moved several times in order to obtain a complete picture of the flow pattern. It is necessary to locate each measurement ‘window’ in relation to the model geometry. For the initial calibration location, where the boundaries are the waterline and the side of the hull, it can be done by locating a plumb bob in the field of view at a known location from the model (the deck edge at each section is the easiest spot to obtain). Subsequent positions can be obtained by knowing how much the measurement frame was moved, but it is desirable to independently check the new location against a known location.

The plumb bob method will not work for a measurement area that is well under the hull. In this case some object must be supported a known distance under the waterline and off the centreline of the hull. The frame used for calibration can be used for this.

EXPERIMENT PREPARATION

This section describes the steps necessary to carry out the PIV experiments on the escort tug model. It is not intended that this is complete, and it is quite likely that some changes will have to be made as experience is gained with the specifics of the PIV system, the model and the test facility.

Model Preparation and Installation

- Mark model with waterline and measurement sections
- Install and check functioning of yaw table
- Install and check functioning of supports for PIV calibration plate
- Lift model (and yaw table) into tank and ballast to correct draft
- Install model under carriage, measurements on downstream side

PIV System Installation

- Assemble support frames on carriage
- Attach PIV system
- Check range of measurements against model (vertical, longitudinal, transverse)
- Check functioning of calibration plate support system in water
- Check functioning of underwater lights, especially under the model

Calibration

- At initial location,
    - Align laser with model at required location
    - Focus cameras on particles within measurement region
    - Align calibration plate with laser
    - Calibrate using visual light (RMS error within tolerance)
    - Check range of frame and centre of frame relative to model

Seeding

- Check functional requirements of seeding system for
    - Measurement location
    - Speeds

PIV System

- Determine optimum sampling parameters for PIV system

Repeat calibration, seeding and PIV system steps after changing model orientation to upstream side and changing PIV system orientation.

TEST SEQUENCE

Proposed test sequence is as follows

Initial yaw angle 20 degrees, PIV system on downstream side of hull, fin removed

Start at section 5 (furthest aft)
Initial location should have frame boundaries given by

- i) Side of model
- ii) Waterline

For this location complete experiments for each speed and repeat with fin fitted.

Move PIV system vertically and repeat until depth requirement has been met at this section.

Reset PIV to waterline and move longitudinally to next section.
Check location of centre of frame relative to model.
Repeat experiments.

Reset PIV (or move model) to obtain next transverse location.

Repeat until all measurements on downstream side are completed.

Change yaw angle and repeat for yaw angle of 45 degrees.

Change from downstream side to upstream side and repeat for yaw angles of 20 and 45 degrees.

Reset PIV and model to centreline plane at midships on downstream side of the model.

CONCLUSIONS

CFD predictions of the forces on an escort tug were compared with experimentally derived values for the same yaw angle range and flow conditions, for the tug with and without a fin. For the case with no fin, the CFD code under estimated the experiment values of sway force by 0.13 N/degree yaw up to 45 degrees of yaw. For the case with the fin, the forces were under predicted by the CFD method by 0.69 N/degree yaw up to yaw angles of 30 degrees. Above this value the experiment and CFD predictions become non-linear. The CFD predictions show the flattening of the sway force component above 40 degrees, even though the magnitude of the force is under-predicted by 18 percent. Below 20 degrees the agreement between the experiment values and the CFD predictions is very good. For surge force, the agreement for the hull only condition is within 2.5N throughout the range of yaw angle. The agreement between the experiment values and the predictions for the cases when the fin was fitted was not as good (within 5 N throughout the range of yaw angle) but this is within the uncertainty of the experiment values.

The CFD predictions show how the fin produces a large vortex, which dramatically increases the level of side force generated by the hull. These predictions, together with earlier experience carrying out PIV experiments in the OERC towing tank, have been used to plan a further set of PIV experiments. The plan has been prepared with the intention of obtaining experiment results that will be suitable for publication is a scientific journal. The plan includes proposed procedures for carrying out the experiments and a method for determining the uncertainty of the PIV system.

REFERENCES

Calagno, G. Di Felice, F., Felli, M, and Pereira, F. ‘Application of Stereo PIV: Propeller Wake Analysis in a Large Circulating Water Channel’, 11th Symposium on Applications of Laser Techniques to Fluid Mechanics, Calouste Gulbenkian Foundation, Lisbon, Portugal, 8th to 11th July, 2002, Paper 26-4.

LaVision GmbH, ‘DaVis FlowMaster Software Manual for DaVis 6.2’, August 2002.

LaVision GmbH, ‘DaVis Software Manual for DaVis 6.2’, January 2004.

Lawson, N. J. and Wu, J. ‘Three-dimensional Particle Image Velocimetry: error Analysis of Stereoscopic Techniques’, *Measurement Science and Technology*, Volume 8, 1997, pp 894-900.

Lawson, N. J. and Wu, J. ‘Three-dimensional Particle Image Velocimetry: Experimental Error Analysis of a Digital Angular Stereoscopic System’, *Measurement Science and Technology*, Volume 8, 1997, pp 1455-1464.

Molyneux, D., ‘A Comparison of Hydrodynamic forces Generated by a VSP Tractor Tug Hull and an ASD Tug Hull, IMD/NRC, TR-2002-16, PROTECTED, November 2002.

Molyneux, D., ‘A Comparison of Flow Measurements Around a Series 60 (C_B=0.6) Hull at Yaw Angles of 10 Degrees and 35 Degrees With CFD Simulations’, IOT/NRC, TR-2005-07, June 2005.

Molyneux, D., and Xu, J. ‘Particle Image Velocimetry Experiments to Measure Flow Around an Escort Tug’, IOT/NRC, TR-2005-10, August 2005.

Soloff, S. M., Adrian, R. J. and Liu, Z-C., ‘Distortion Compensation for Generalized Stereoscopic Particle Image Velocimetry’, *Measurement Science and Technology*, Volume 8, 1997, pp 1441-1454.

Xu, J., Molyneux, D. and Bose, N., ‘A Versatile Particle Image Velocimetry System for Flow Measurements in Water Tanks’, 7th Canadian Marine Hydromechanics and Structures Conference, Halifax, N. S. September 2005.